

# Engineered T cell therapy for central nervous system injury



<https://doi.org/10.1038/s41586-024-07906-y>

Received: 16 January 2023

Accepted: 5 August 2024

Published online: 4 September 2024

 Check for updates

Wenqing Gao<sup>1,2,8</sup>, Min Woo Kim<sup>1,2,3,4,8</sup>, Taitea Dykstra<sup>1,2</sup>, Siling Du<sup>1,2,3</sup>, Pavle Boskovic<sup>1,2</sup>, Cheryl F. Lichti<sup>2,5</sup>, Miguel A. Ruiz-Cardozo<sup>6</sup>, Xingxing Gu<sup>1,2</sup>, Tal Weizman Shapira<sup>7</sup>, Justin Rustenhoven<sup>1,2</sup>, Camilo Molina<sup>6</sup>, Igor Smirnov<sup>1,2</sup>, Yifat Merbl<sup>7</sup>, Wilson Z. Ray<sup>8</sup> & Jonathan Kipnis<sup>1,2,3,4</sup>

Traumatic injuries to the central nervous system (CNS) afflict millions of individuals worldwide<sup>1</sup>, yet an effective treatment remains elusive. Following such injuries, the site is populated by a multitude of peripheral immune cells, including T cells, but a comprehensive understanding of the roles and antigen specificity of these endogenous T cells at the injury site has been lacking. This gap has impeded the development of immune-mediated cellular therapies for CNS injuries. Here, using single-cell RNA sequencing, we demonstrated the clonal expansion of mouse and human spinal cord injury-associated T cells and identified that CD4<sup>+</sup> T cell clones in mice exhibit antigen specificity towards self-peptides of myelin and neuronal proteins. Leveraging mRNA-based T cell receptor (TCR) reconstitution, a strategy aimed to minimize potential adverse effects from prolonged activation of self-reactive T cells, we generated engineered transiently autoimmune T cells. These cells demonstrated notable neuroprotective efficacy in CNS injury models, in part by modulating myeloid cells via IFN $\gamma$ . Our findings elucidate mechanistic insight underlying the neuroprotective function of injury-responsive T cells and pave the way for the future development of T cell therapies for CNS injuries.

Among the complex milieu of immune cells that percolate through the CNS following injury, T cells have roles that have been reported to either exacerbate damage<sup>2</sup> or promote neuronal survival<sup>3,4</sup>. In fact, previous studies have demonstrated that CD4<sup>+</sup> T cells reactive to myelin proteins could improve neuronal survival after CNS injury<sup>3</sup>, despite their potential to induce CNS autoimmunity<sup>5,6</sup>. However, the mechanisms through which these autoimmune T cells exert their neuroprotective effects remain poorly understood.

T cell-based immunotherapy is currently at the forefront of cancer treatments. A commonly used approach uses antibodies to checkpoint inhibitors, such as PD1 or CTLA4, which normally limit immune cell-mediated tumour rejection<sup>7</sup>. A more targeted approach uses the ex vivo generation of autologous artificial T cells whose surfaces bear chimeric antigen receptors (CARs) towards tumour antigens<sup>8</sup>. Although the implementation of checkpoint immunotherapy and of CAR T cells largely work through cytotoxic CD8<sup>+</sup> T cells, similar approaches could be utilized in other pathologies, such as CNS injury, to harness specific T cell populations for clinical benefit<sup>3</sup>. To date, however, neither the transcriptional characteristics nor the antigen specificities of injury-associated neuroprotective T cells have been identified. Moreover, as injury-associated T cells are likely to be directed towards CNS self-antigens presented at the injury site, uncontrolled or prolonged expansion of these self-reactive T cells may elicit devastating autoimmune responses<sup>9</sup>.

In this study, we utilized single-cell TCR sequencing of T cells obtained from the site of contusion after spinal cord injury (SCI). Injury-associated TCRs were then cloned and reconstituted into primary autologous CD4<sup>+</sup> T cells. Peripheral administration of these T cells expressing reconstituted TCRs demonstrated neuroprotective effects in two different models of CNS injury: optic nerve injury (ONI) and SCI. Antigen specificity guided the migration of neuroprotective T cells to the injury site, where they shaped both microglia and macrophage phenotypes in an IFN $\gamma$ -dependent manner. To avoid the risk of triggering detrimental autoimmune responses in the long term, we utilized mRNA-based transient TCR expression in mouse primary T cells. These engineered transient autoimmune (ETA) T cells replicated the neuroprotective effects in both ONI and SCI. Clonal expansion of T cells was also detected in the cerebrospinal fluid (CSF) of patients with SCI. Together, these findings contribute to our understanding of endogenous mechanisms underlying T cell-dependent neuroprotection after CNS injury.

## Clonality of CNS-infiltrating T cells after SCI

Following SCI, astrocytes form a glial scar around the injury site marked by the absence of the glial fibrillary acid protein (GFAP) signal<sup>10</sup>. Consistent with previous reports<sup>11</sup>, we observed an accumulation of immune cells, including T cells, at the injury site of the spinal cord parenchyma

<sup>1</sup>Center for Brain Immunology and Glia (BIG), Washington University in St. Louis, School of Medicine, St. Louis, MO, USA. <sup>2</sup>Department of Pathology and Immunology, Washington University in St. Louis, School of Medicine, St. Louis, MO, USA. <sup>3</sup>Immunology Program, School of Medicine, Washington University in St. Louis, School of Medicine, St. Louis, MO, USA. <sup>4</sup>Medical Scientist Training Program, School of Medicine, Washington University in St. Louis, School of Medicine, St. Louis, MO, USA. <sup>5</sup>Bursky Center for Human Immunology and Immunotherapy Programs, Washington University in St. Louis, School of Medicine, St. Louis, MO, USA. <sup>6</sup>Department of Neurological Surgery, Washington University in St. Louis, School of Medicine, St. Louis, MO, USA. <sup>7</sup>Systems Immunology Department, The Weizmann Institute of Science, Rehovot, Israel. <sup>8</sup>These authors contributed equally: Wenqing Gao, Min Woo Kim. <sup>✉</sup>e-mail: gaow@wustl.edu; kipnis@wustl.edu

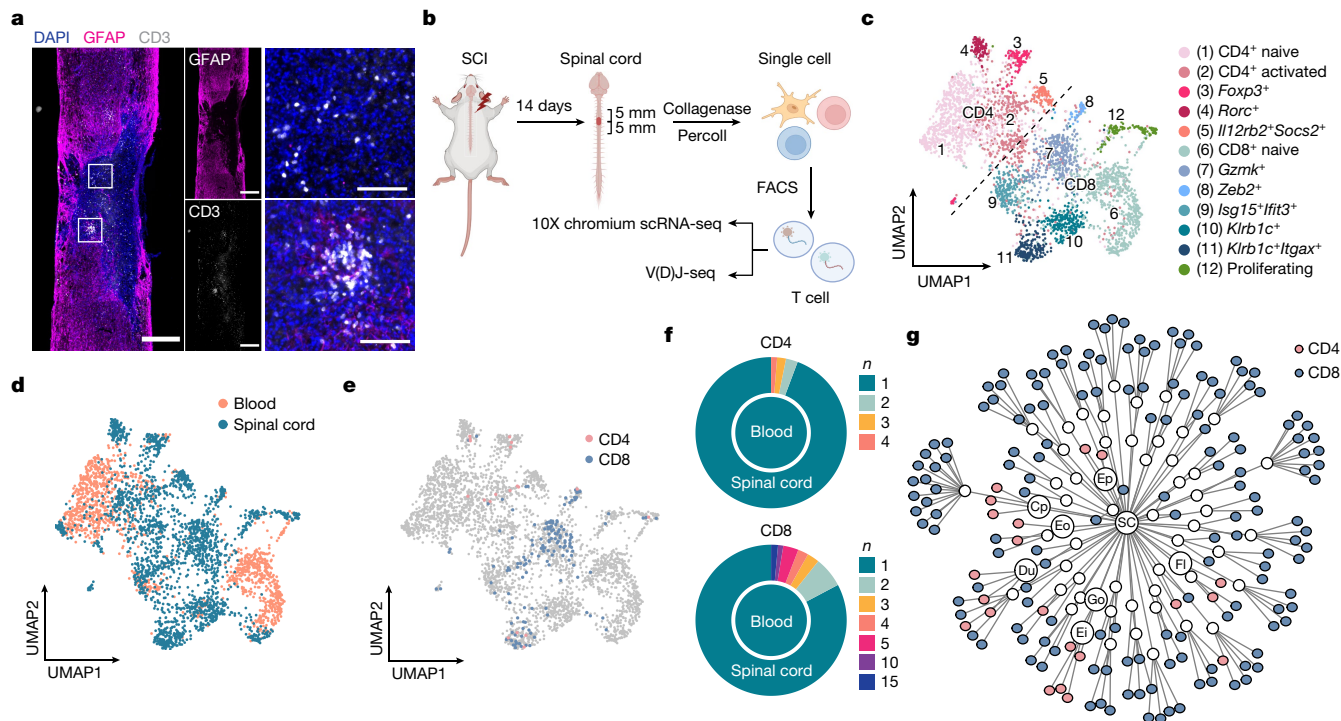


**Fig. 1 | Clonality of T cells after CNS injury.** **a**, Immunohistochemistry of the GFAP injury site and CD3<sup>+</sup> T cell infiltration 14 days after SCI. The insets represent enlarged areas of interest. Experiments were repeated at least twice. Scale bars, 500  $\mu$ m and 100  $\mu$ m (insets). **b**, Schematic representation of T cell isolation and scRNA-seq from an injured spinal cord. Data from two independent experiments were combined.  $n = 30$  mice were used for T cell isolation from injured spinal cords based on DAPI<sup>+</sup> CD45<sup>+</sup> Thy1.2<sup>+</sup> CD4<sup>+</sup>/CD8<sup>+</sup> FACS. The diagram was created using BioRender (<https://biorender.com>). **c**, UMAP visualization of T cell populations from injured spinal cord and homeostatic

blood of naive mice based on marker gene expression. **d**, UMAP visualization of T cell populations from injured spinal cord or homeostatic blood colour-coded by sample. **e**, UMAP visualization of T cell clonality. Cells with shared sequences of the CDR3 region of both the TCR $\alpha$  chain and the TCR $\beta$  chain are defined as a TCR clone. **f**, Pie graphs showing the proportions of CD4<sup>+</sup> and CD8<sup>+</sup> T cell clones in injured spinal cord or homeostatic blood. **g**, Q-plot visualization of information for each TCR clone (dots in white) and cells (dots with colour) sharing the same TCR sequences based on the CD4<sup>+</sup> or CD8<sup>+</sup> T cell subtype. CD4<sup>+</sup> T cell clones are highlighted.

and spinal cord meninges after SCI (Fig. 1a and Extended Data Fig. 1a,b). To further investigate the phenotype and potential clonal expansion, we sorted these injury-associated T cells from the SCI site and profiled them using the 10X genomics chromium gene expression and V(D)J sequencing platform (Fig. 1b). T cells isolated from the blood of naive mice served as controls. Unsupervised clustering and dimensionality reduction using uniform manifold approximation and projection (UMAP) revealed 12 different T cell subclusters (Fig. 1c and Extended Data Fig. 1c). Whereas most T cells isolated from the blood of uninjured mice were classified as naive, most T cells recovered from the injured spinal cords displayed, as expected, transcriptional signatures suggestive of activation and differentiation (Fig. 1d and Extended Data Fig. 1d–h).

TCRs determine the antigen specificity of T cells. Functional TCR complexes are assembled by TCR $\alpha$  and TCR $\beta$  chains, together with the CD3 complex. During T cell development, V(D)J recombination assembles TCR gene segments in a nearly random manner, ensuring TCR diversity. Our analysis of T cells from injured spinal cords revealed enrichment in specific TCR $\alpha$  subtypes (for example, TRAV1 and TRAV13), but not in any specific TCR $\beta$  subtype (Extended Data Fig. 2a,b). Whereas complementarity-determining region 1 (CDR1) and CDR2 of the variable TCR $\alpha$  and TCR $\beta$  chains mostly contribute to interactions with major histocompatibility complex (MHC), CDR3 is the most diverse region and often dictates antigen specificity. To explore whether CNS-infiltrating T cells represent expanded clonotypes, we analysed their CDR3 sequences. Cells exhibiting shared CDR3 sequences of TCR $\alpha$  and TCR $\beta$  pairs are defined as T cell clones. Whereas blood samples from naive mice revealed no T cell clonality (as expected of a non-infected mouse), after SCI, both CD8<sup>+</sup> and CD4<sup>+</sup> exhibited

clonal expansion at the injury site (Fig. 1e–g). The majority of CD8<sup>+</sup> T cell clones observed in the injured spinal cord were present in clusters with high granzyme expression, suggesting a cytotoxic phenotype, whereas CD4<sup>+</sup> T cell clones displayed diverse phenotypes (Fig. 1e and Extended Data Fig. 2c,d). There was also a higher proportion of invariant natural killer T (TRAV11<sup>+</sup>) cells in the injured spinal cord than in blood, attributable to their tissue-homing nature<sup>12</sup> (Extended Data Fig. 2a,b); however, no clonal expansion was observed within this population.

### Neuroprotective function of CD4<sup>+</sup> T cells

Self-reactive T cells, such as those targeting myelin proteins, exist in healthy mice and humans, owing to incomplete central tolerance or cross-reactivity with microbiota-derived or food-derived components that share similarity with self-derived antigens<sup>13–15</sup>. In fact, these self-reactive T cells persist through peripheral tolerance<sup>16</sup>, yet their physiological function is not completely understood. As exogenously injected autoimmune T cells demonstrated neuroprotection after CNS injury, we hypothesized that endogenous T cells, clonally expanding in response to CNS injury, are also self-reactive and that they bear neuroprotective properties.

We utilized a short-term and robust ONI model to screen the function of injury-associated T cells. After ONI, immune cells, including T cells, are found within the ONI site (Extended Data Fig. 3a). ONI results in a quantifiable loss of retinal ganglion cells (RGCs), which is the cell body of optic nerve axons and can be used to assess the effect of T cell treatment (Extended Data Fig. 3b). First, to reproduce previously published works, suggesting that autoreactive T cells are neuroprotective, we isolated CD4<sup>+</sup> T cells from TCR transgenic mice expressing

myelin oligodendrocyte glycoprotein 35–55-specific (MOG<sub>35–55</sub>; 2D2 mice) or the chicken ovalbumin 323–339-specific (OVA<sub>323–339</sub>; OT-II mice) TCRs. T cells from wild-type (WT) mice were used as controls. T cells were activated *in vitro* and injected intravenously into mice immediately after ONI (Extended Data Fig. 3c,d). Compared with OVA-reactive T cells or polyclonal T cells from WT mice, MOG-reactive T cells accumulated in the injured optic nerve in both females and males (Extended Data Fig. 3e,g). Consistent with this, the survival of RGCs improved in MOG-reactive T cell recipients of both sexes (Extended Data Fig. 3f,h). Although bystander T cell recruitment to the injury site could be observed (Extended Data Fig. 3i–k), recovery from ONI was most pronounced with the delivery of MOG-reactive T cells.

Using the self-cleaving peptide P2A to link TCR $\alpha$  and TCR $\beta$ , we used a retrovirus infection system to introduce TCRs into primary T cells<sup>17</sup> (Extended Data Fig. 4a). To confirm that this approach results in functional TCRs, we assessed the proliferative capacity of primary T cells with known reconstituted TCRs (2D2 recognizing MOG<sub>35–55</sub>, and OT-II recognizing OVA<sub>323–339</sub>) towards their respective cognate antigens (Extended Data Fig. 4b). When treating mice with ONI with T cells expressing reconstituted TCR<sub>2D2</sub>, we observed similar neuroprotection as with T cells isolated from the TCR transgenic mice above (Extended Data Fig. 4c,d).

We then utilized the same strategy to reconstitute TCRs of all effector CD4<sup>+</sup> T cell clones identified by V(D)J sequencing from the injured CNS. With three rounds of independent screening, we tested a total of six injury-associated CD4<sup>+</sup> effector T cell clones and identified three TCRs (Cp, Du and Go) that led to improved recovery after ONI (Extended Data Fig. 4c–f). No beneficial effect could be observed when treating mice with ONI with T cells expressing TCRs from blood T cells (Extended Data Fig. 4g), clonally expanded spinal cord CD8<sup>+</sup> T cells (although detrimental effects were obtained with TCR<sub>Ak</sub> CD8<sup>+</sup> T cells; Extended Data Fig. 4h) or T cells expressing a diaphragm-enriched TCR<sub>Dl</sub> (Extended Data Fig. 4i).

Of note, T cells expressing TCR<sub>Cp</sub> and TCR<sub>Du</sub> exhibited higher clonality than any other injury-associated CD4<sup>+</sup> T cell clone, suggesting a potential correlation between clonal expansion and neuroprotective function (Fig. 1g and Extended Data Fig. 4e,f). Moreover, retrograde tracing with Fluoro-Gold injection into the superior colliculus (Extended Data Fig. 4j) also demonstrated an increase in viable RGCs after ONI with intravenous injection of either TCR<sub>Cp</sub> or TCR<sub>Du</sub>, further confirming their neuroprotective function (Extended Data Fig. 4k).

Having identified TCR<sub>Cp</sub> and TCR<sub>Du</sub> as promising TCR candidates in ONI, we assessed the neuroprotective capacity of these clones after SCI. As SCI represents a more complex insult with a prolonged recovery phase, we injected TCR-expressing T cells twice, first immediately after the injury and again 3 days later, and then measured locomotion recovery using the Basso Mouse Scale (BMS)<sup>18</sup> (Fig. 2a). Compared with control mice (no T cell treatment), treatment with T cells expressing TCR<sub>Cp</sub> exhibited a beneficial effect following SCI, whereas treatment with T cells expressing TCR<sub>OT-II</sub> or diaphragm-enriched TCR<sub>Dl</sub> did not have any significant effect on recovery (Fig. 2b and Extended Data Fig. 4l). Treatment with the T cells expressing TCR<sub>Du</sub>, although neuroprotective in ONI, yielded no improvement after SCI (Fig. 2b).

Regardless of the reconstituted TCRs, T cells exhibited a T helper 1 (T<sub>H1</sub>)-like phenotype when cultured *in vitro* (Extended Data Fig. 5a). Furthermore, when T cells expressing injury-associated TCRs were assessed at the injury site upon injection into tissue from mice with SCI, they maintained the T<sub>H1</sub> phenotype (Extended Data Fig. 5b–e). We next sought to determine whether the tissue microenvironment altered the phenotype of T cells at the injury site. To this end, SCI was induced in mice, followed by injection of T cells with retroviral-driven TCR<sub>Cp</sub> and GFP expression. After 14 days, GFP<sup>+</sup> T cells were isolated from both the injured spinal cord and the spleen and were subjected to single-cell RNA sequencing (scRNA-seq) analysis (Extended Data Fig. 5f). T cells demonstrated tissue-specific clustering via UMAP dimensionality

reduction, suggesting phenotypic alterations (Extended Data Fig. 5g). Compared with TCR<sub>Cp</sub>-expressing T cells isolated from the spleen, those isolated from the injured spinal cord exhibited higher expression levels of genes associated with transcription, translation, vesicle trafficking and IFN $\gamma$  production, indicative of a more activated state (Extended Data Fig. 5h,i). Gene signatures revealed that TCR<sub>Cp</sub>-expressing T cells isolated from the injured spinal cord exhibited a T<sub>H1</sub> or T<sub>H1</sub> memory phenotype, whereas those in the spleen exhibited a T follicular helper phenotype<sup>19,20</sup> (Extended Data Fig. 5j–l). Thus, antigen specificity guides the accumulation of injury-associated T cells to the injury site, with the local microenvironment maintaining these T cells in a T<sub>H1</sub> state.

SCI damages the myelin sheath, neurons and astrocytes, whereas microglia and peripheral immune cells accumulate at the injury site (Fig. 1a and Extended Data Fig. 6a,b). On the basis of previous studies on tissue repair macrophages<sup>21</sup>, we hypothesized that T cells might tune the local inflammatory response, thereby limiting secondary neurodegeneration. To test this possibility, we performed scRNA-seq of total CD45<sup>+</sup> immune cells isolated from the injury site of mice with SCI treated with TCR<sub>Cp</sub> T cells compared with control mice with SCI (Fig. 2c). Phenotyping these CD45<sup>+</sup> populations revealed that microglia and macrophages represented the two major myeloid populations at the injury site after SCI. Monocytes, dendritic cells, neutrophils, T cells and B cells (along with contaminating CD45<sup>+</sup> populations of fibroblasts and endothelial cells) were also observed. Treatment with TCR<sub>Cp</sub> T cells reduced macrophage infiltration as well as both proliferating macrophages and microglia at the injured spinal cord (Fig. 2d,e and Extended Data Fig. 6c,d). Delving deeper into these changes, we subclustered both the macrophage and the microglial populations to determine their responses to the injected T cells. Microglia were subclustered as homeostatic, transition, activated or IFN-responsive microglia. Treatment of mice with SCI with TCR<sub>Cp</sub> T cells induced a substantial reduction in inflammatory, activated microglia and increased frequencies of homeostatic and IFN-responsive microglia (Fig. 2f,g and Extended Data Fig. 6e). Macrophages were also subclustered as inflammatory, anti-inflammatory, chemotactic, border-associated, angiogenic, MHC-II<sup>+</sup> or IFN-responsive macrophages. Treatment with TCR<sub>Cp</sub> T cells attenuated the frequency of inflammatory macrophages, increasing the proportions of other subclusters (Fig. 2h,i and Extended Data Fig. 6f). Although fibroblasts were contaminants resulting from incomplete CD45<sup>+</sup> cell purification, the numbers that we obtained sufficed for analysis of their gene ontology pathways, where we observed upregulation of pathways involved in wound healing and downregulation of pathways involved in inflammation (Extended Data Fig. 6g,h).

To identify molecules that modulate the local immune response, we performed ligand–receptor analysis to examine which pathways responding to T cell signalling changed after T cell treatment. Several pathways, including IFN $\gamma$ -responsive, IL-2-responsive and TGF $\beta$ 1-responsive pathways, demonstrated differences, with the IFN $\gamma$ -responsive pathways showing the most pronounced changes in microglial and macrophage populations (Extended Data Fig. 6i). Although IFN $\gamma$  is generally considered a pro-inflammatory cytokine, exhibiting pleiotropic effects on macrophages, T cells and other cell types, studies exist supporting its anti-inflammatory properties in CNS pathology<sup>22–24</sup>. Indeed, both the dose and the context for which IFN $\gamma$  signalling occurs determines its protective function in experimental autoimmune encephalomyelitis as well as in CNS injury<sup>25–27</sup>. Recent literature has further illustrated the complex biology of IFN $\gamma$  signalling that could lead to both pro-inflammatory and anti-inflammatory responses on target cells<sup>28–30</sup>. Moreover, the function of IFN $\gamma$  in promoting scar formation through fibroblasts during neuroinflammation has also been reported<sup>31</sup>. We found that TCR<sub>Cp</sub> T cells had the ability to secrete IFN $\gamma$ , and blocking their production of IFN $\gamma$  by generating TCR<sub>Cp</sub> T cells on a *Ifng*<sup>-/-</sup> background interfered with their neuroprotective capacity (Fig. 2j,k). Given that TCR<sub>Cp</sub> *Ifng*<sup>-/-</sup> T cells could recruit endogenous T cells, which may produce IFN $\gamma$ , we used IFN $\gamma$  neutralizing antibody treatment or performed SCI on *Ifng*<sup>-/-</sup> mice and



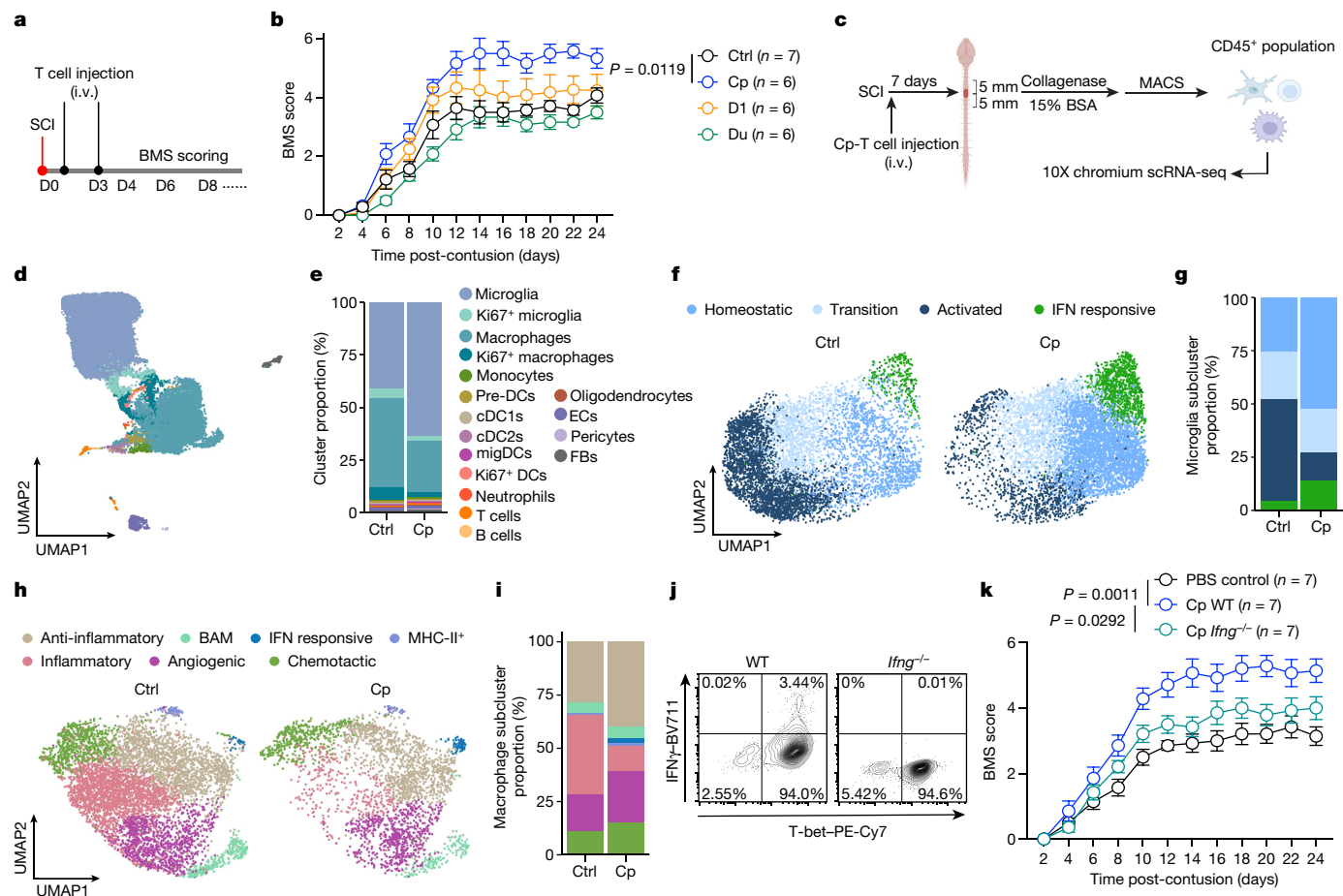


**Fig. 2 | Neuroprotective function of injury-associated T cells after CNS injury.** **a**, Schematic representation of the SCI model to test the neuroprotective function of T cells. D0, day 0; i.v., intravenous. **b**, The BMS score of mice after SCI and injections with CD4<sup>+</sup> T cells expressing retrovirus-delivered TCRs, with PBS treatment after injury as control (ctrl). Data are presented as mean ± s.e.m. Two-way analysis of variance (ANOVA) with Tukey's post-hoc test were used. **c**, Schematic representation of the isolation and scRNA-seq analysis of CD45<sup>+</sup> cell populations from the injury site of mice with SCI treated with CD4<sup>+</sup> T cells carrying TCR<sub>Cp</sub> or treated with PBS as a control. For each group, *n* = 4 mice were pooled for the isolation of the CD45<sup>+</sup> cell population. MACS, magnetic-activated cell sorting. The diagram was created using BioRender (<https://biorender.com>). **d**, UMAP visualization of scRNA-seq analysis of cell populations after SCI based on cell types. **e**, Bar graph showing cluster proportions of each cell cluster

separately. cDC1, conventional type 1 dendritic cell; DC, dendritic cell; EC, endothelial cell; FB, fibroblast; migDC, migratory DC. **f**, UMAP visualizations of four subclusters of microglia in control and TCR<sub>Cp</sub> groups. **g**, Bar graph showing subcluster proportions of microglia in each group. **h**, UMAP visualizations of seven subclusters of macrophages in control and TCR<sub>Cp</sub> groups. BAM, border-associated macrophage. **i**, Bar graph showing subcluster proportions of macrophages in each group. **j**, Flow cytometry analysis of in vitro-cultured TCR<sub>Cp</sub>-expressing CD4<sup>+</sup> T cells from WT or *Ifng*<sup>-/-</sup> mice before injection. **k**, BMS score of mice after SCI and injections with TCR<sub>Cp</sub>-expressing CD4<sup>+</sup> T cells isolated from WT or *Ifng*<sup>-/-</sup> mice, with PBS treatment after injury as control. Data are presented as mean ± s.e.m. Two-way ANOVA with Tukey's multiple comparison test were used.

treated them with TCR<sub>Cp</sub> T cells. The neuroprotective effect of injected T cells was blocked (Extended Data Fig. 6j,k). Collectively, these results demonstrate that neuroprotective T cells tune local immune responses by decreasing the inflammatory contributions of microglia and infiltrating macrophages through IFN $\gamma$ .

### Antigen specificity of injury-associated CD4<sup>+</sup> T cells

We sought to identify the antigen specificity of injury-associated T cells. To enable antigen screening of injury-associated CD4<sup>+</sup> T cells, we utilized the 58 $\alpha$ -58 $\beta$ -NFAT-GFP reporter system – a T cell hybridoma lacking endogenous TCR – combined with a retrovirus infection system that allows expression of exogenous TCRs<sup>32,33</sup>. These hybridoma cells with reconstituted TCRs were then co-cultured with antigen-presenting cells (APCs) and antigen candidates to assess for reactivity by both IL-2 secretion and NFAT-dependent GFP expression (Fig. 3a). We first tested a panel of immunogenic CNS-derived peptides and found that many of our injury-associated CD4<sup>+</sup> T cell clones (Du, Eo, Fl and Go) recognized

the myelin peptide, MOG<sub>35–55</sub>, in a dose-dependent manner, confirming reactivity of endogenous injury-associated TCRs to CNS-specific antigens (Fig. 3b–d and Extended Data Fig. 7a,b). To further verify their specificity, we co-cultured these hybridomas in the presence of MOG<sub>45–64</sub>, representing a shifted binding register, and found that it failed to adequately activate the hybridomas (Fig. 3c,d). Moreover, mutation of MOG<sub>35–55</sub> at key residues within its minimal binding epitope<sup>34</sup>, affecting TCR response but not MHC-II binding, resulted in complete loss of hybridoma activation, substantiating Du/Eo/Fl/Go specificity towards MOG<sub>35–55</sub> (Extended Data Fig. 7a,b). Deletion of MHC-II expression on APCs also blocked MOG<sub>35–55</sub>-induced activation of hybridoma Du/Eo/Fl/Go (Extended Data Fig. 7c,d). Although the magnitudes of their responses were lower than the well-established self-reactive TCR<sub>2D2</sub>, they appeared to be specific to MOG<sub>35–55</sub>.

We continued to explore the antigen specificity of TCR<sub>Cp</sub> T cells. The antigen epitopes recognized by CD4<sup>+</sup> T cells need to be processed and presented by APCs on MHC-II molecules. By isolating the MHC-II complex via immunoprecipitation and profiling peptide sequences



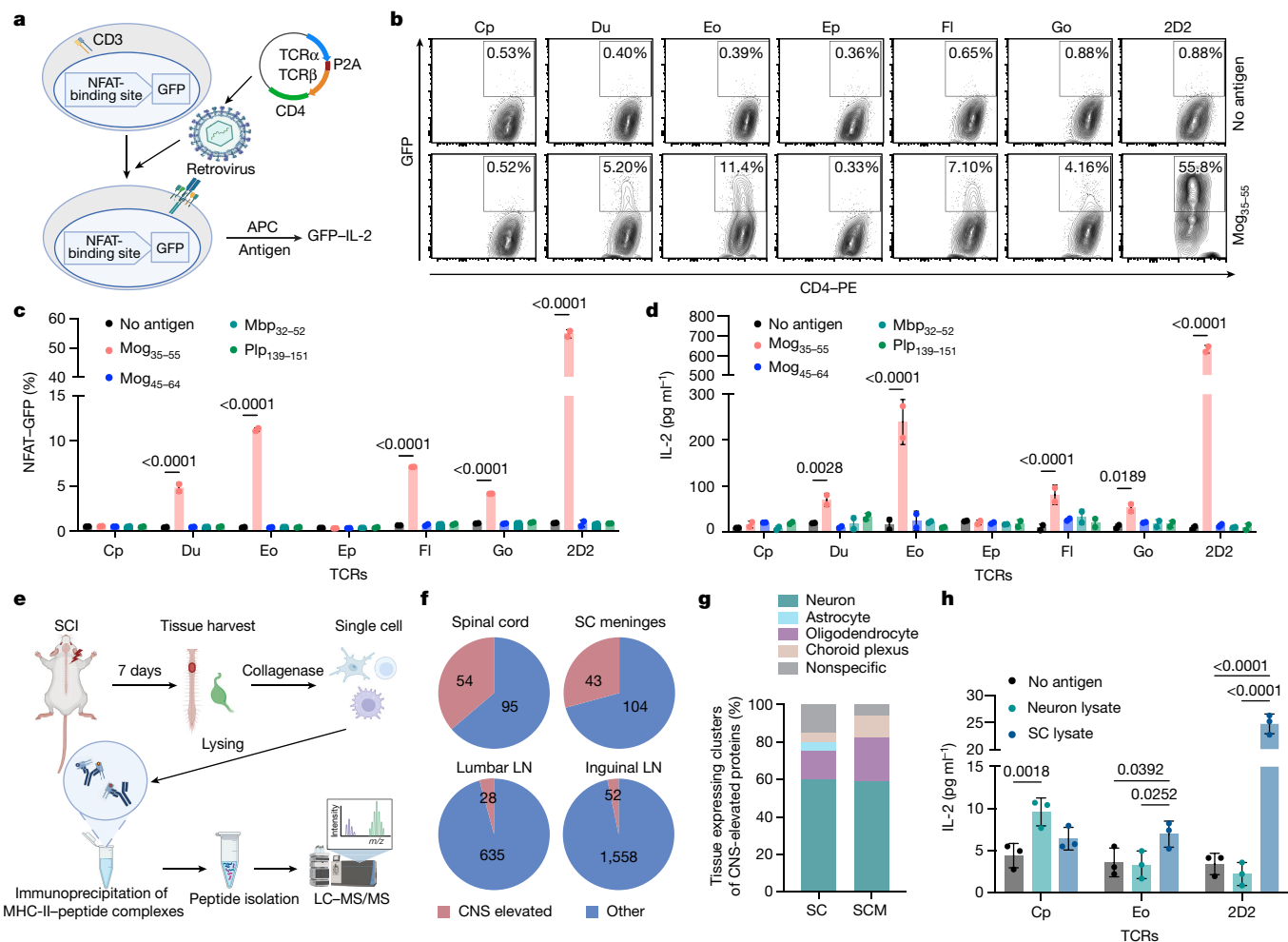


**Fig. 3 | Antigen specificity of self-reactive T cells.** **a**, Schematic representation of the NFAT-GFP hybridoma reporter system to test the antigen specificity of each TCR. **b**, Flow cytometry analysis of NFAT-GFP reporter activation in hybridomas expressing specific TCRs after co-culturing with APCs and 5  $\mu$ M of MOG<sub>35-55</sub> peptide. **c, d**, Flow cytometry quantification (**c**) and IL-2 ELISA (**d**) showing hybridoma activation after co-culturing with APCs and 5  $\mu$ M of different peptides. Experiments were repeated at least three times, and one representative result is shown. Data are represented as mean  $\pm$  s.d.,  $n = 2$  technical replicates. Two-way ANOVA with Tukey's multiple comparison test were used. **e**, Schematic depicting the identification of MHC-II-binding peptides in the injured spinal cord. Spinal cords (and other indicated tissues) from  $n = 50$  total mice were pooled 7 days after SCI for MHC-II immunoprecipitation. The diagrams in panels a and e were created using BioRender (https://biorender.com).

LC-MS/MS, liquid chromatography-tandem mass spectrometry. **f**, Pie graphs showing the proportions and number of CNS-elevated peptides in the total MHC-II-binding peptidome of each tissue. CNS-elevated peptides were identified based on the Human Protein Atlas database (translated Uniprot ID from human to mouse). LN, lymph node. **g**, Bar graph showing the proportion of tissue-expressing clusters of CNS-elevated proteins included in the MHC-II peptidome in the injured spinal cord or spinal cord meninges (SCMs; dura mater). **h**, ELISA quantification showing IL-2 secretion by reporter hybridomas expressing specific TCRs after co-culturing with APCs and either no antigen (control), primary neuronal lysate (1 mg wet pellet ml<sup>-1</sup>), or spinal cord lysate (500  $\mu$ g wet pellet ml<sup>-1</sup>). Experiments were repeated twice, and one representative result is shown. Data are represented as mean  $\pm$  s.d.,  $n = 3$  technical replicates. Two-way ANOVA with Tukey's multiple comparison test were used.

via mass spectrometry, we sought to identify a pool of self-peptides presented on MHC-II, representing potential candidates for therapeutic TCR recognition<sup>35</sup>. We collected samples from 50 mice with SCI, performed MHC-II immunoprecipitation and conducted peptide mass spectrometry (Fig. 3e). A total of 296 different self-peptides were detected in the injured spinal cord sample and its associated meningeal dura mater (Supplementary Table 1). By translating UniProt IDs of our identified peptides to their human equivalents and aligning these with the Human Protein Atlas database (https://www.proteinatlas.org), we grouped our peptide targets as 'CNS-elevated' or 'others' (Fig. 3f). Shared or distinct CNS-elevated MHC-II-bound proteins in the spinal cord and its meninges are listed (Extended Data Fig. 7e and Supplementary Table 2). Despite testing a pool of CNS-elevated MHC-II-bound peptides, none of them reliably activated TCR<sub>Cp</sub> T cells in vitro. In addition, Protein Modification Integrated Search Engine (PROMISE) analysis<sup>36</sup> showed that post-translational modifications

generally exist on peptides from the MHC-II-binding peptidome (Supplementary Table 3), increasing the challenge for antigen exploration. As most MHC-II-bound peptides detected by mass spectrometry belong to proteins derived from neurons (Fig. 3g), we tested the possibility of TCR<sub>Cp</sub> T cells recognizing neuronal peptides. Co-culturing TCR<sub>Cp</sub> hybridomas with APCs and primary neuron lysate induced their activation, whereas MOG-specific hybridomas responded to myelin-rich spinal cord lysate (Fig. 3h and Extended Data Fig. 7f, g). Future studies should focus on improving methodologies to more readily identify the antigen specificity of neuroprotective T cells, which will facilitate the development of therapeutic modalities for patients.

### mRNA-based engineered T cell therapy for CNS injury

To minimize potential long-term side effects of self-reactive T cells, we used mRNA transfection (via electroporation) of primary CD4<sup>+</sup>

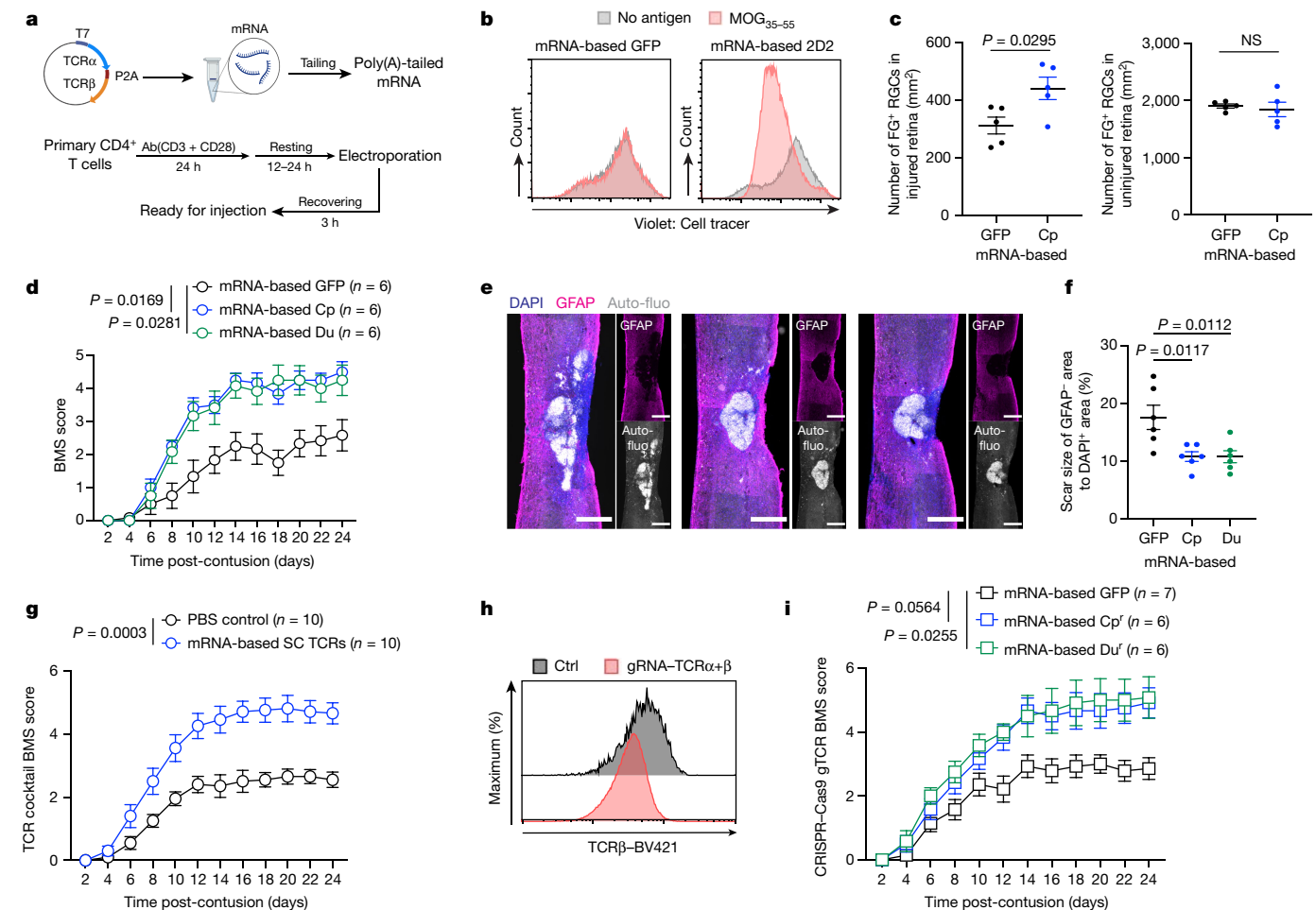


**Fig. 4 | mRNA-TCR-based T cell therapy for CNS injury.** **a**, Schematic representation of transient TCR reconstitution in primary CD4<sup>+</sup> T cells by mRNA electroporation. Ab, antibody. The diagram was created using BioRender (<https://biorender.com>). **b**, T cell proliferation assay to test the function of transiently reconstituted TCRs using Cell Tracer Violet dilution. **c**, Quantification of Fluoro-Gold (FG<sup>+</sup>) RGCs in the injured (ipsilateral) and uninjured (contralateral) retinas after ONI and treatment with CD4<sup>+</sup> T cells expressing mRNA-based GFP or TCR<sub>Cp</sub>. *n* = 5 mice per group. Data are presented as mean ± s.e.m. Two-tailed unpaired Student's *t*-test was used. NS, not significant. **d**, BMS score of mice after SCI and treatment with CD4<sup>+</sup> T cells expressing the indicated mRNA-based TCRs. Data are presented as mean ± s.e.m. Two-way ANOVA with Tukey's multiple comparison test were used. **e**, Immunohistochemistry of the scar region of injured mouse spinal cords after treatment with CD4<sup>+</sup> T cells expressing mRNA-based GFP (left), TCR<sub>Cp</sub> (middle), or TCR<sub>Du</sub> (right). Scale bars, 500 μm.

**f**, Quantification of scar size measured as the percentage of the GFAP<sup>+</sup> area out of all the DAPI<sup>+</sup> area. *n* = 6 mice per group. Data are presented as mean ± s.e.m. One-way ANOVA with Tukey's multiple comparison test were used. **g**, BMS score of mice after SCI and treatment with PBS or CD4<sup>+</sup> T cell cocktails expressing mRNA-based TCRs from the injured spinal cord (Cp, Du and Eo). Data are presented as mean ± s.e.m. Two-way ANOVA with Sidak's multiple comparison test were used. **h**, Flow cytometry analysis for endogenous TCR removal 3 days after delivering guide RNA targeting endogenous TCRs to T cells isolated from Cas9 transgenic mice using a retrovirus vector. **i**, BMS score of mice with SCI after injury and T cell injection. T cells were primary CD4<sup>+</sup> T cells with endogenous TCR removed, expressing mRNA-based GFP or CRISPR-Cas9-resistant TCR<sub>Cp</sub> or TCR<sub>Du</sub>. Data are presented as mean ± s.e.m. Two-way ANOVA with Tukey's multiple comparison test were used.

T cells to generate a transient TCR expression system (Fig. 4a). This method resulted in the short-term expression of the injury-associated TCRs (Extended Data Fig. 8a,b), creating ETA T cells. Similar to retroviral-based TCR delivery, most of the T cells with mRNA-delivered TCRs exhibited a T<sub>H</sub>1-like phenotype regardless of the TCR expressed (Extended Data Fig. 8c). Assays of T cell proliferation in response to their cognate antigens confirmed the functionality of mRNA-based TCR delivery (Fig. 4b). We first tested our putative ETA T cell therapy in the ONI model, where we observed a neuroprotective effect by TCR<sub>Cp</sub> ETA T cells (Fig. 4c). With this observation, we turned our attention back to SCI. In contrast to the results observed with stable TCR expression, transient delivery via mRNA-based electroporation – and therefore with minimal autoimmune side effects – resulted in a strong protective effect after SCI in both TCR<sub>Cp</sub> T cells and TCR<sub>Du</sub> T cells (Fig. 4d and Supplementary Video 1). The protective effect of ETA T cell therapy was evident not only from the improved locomotion

indicated by the BMS score but also from the histopathological finding of a reduced GFAP scar size at the injury site (Fig. 4e,f). In addition, an attenuated distribution of CD45<sup>+</sup> immune cells and a more contained GFAP scar at the injury site suggested a dampened inflammatory response, consistent with data from CD45<sup>+</sup> sequencing (Fig. 4e and Extended Data Fig. 8d). The neuroprotective effect of TCR<sub>Cp</sub> ETA T cells was also IFN $\gamma$  dependent (Extended Data Fig. 8e). We next used our mRNA-based TCR expression strategy to express other MOG-reactive TCRs (Eo, Go and 2D2) and tested their effect after SCI, in which we also observed a protective function of these MOG-reactive TCRs (Extended Data Fig. 8f).

Considering the limited time frame for potential clinical implementation of cell therapy after SCI, we tested the time window for functional T cell treatment. Injection of therapeutic T cells 1 day after injury provided effective protection; some mice still responded to T cells injected 7 days after injury. However, the proportion of responding animals

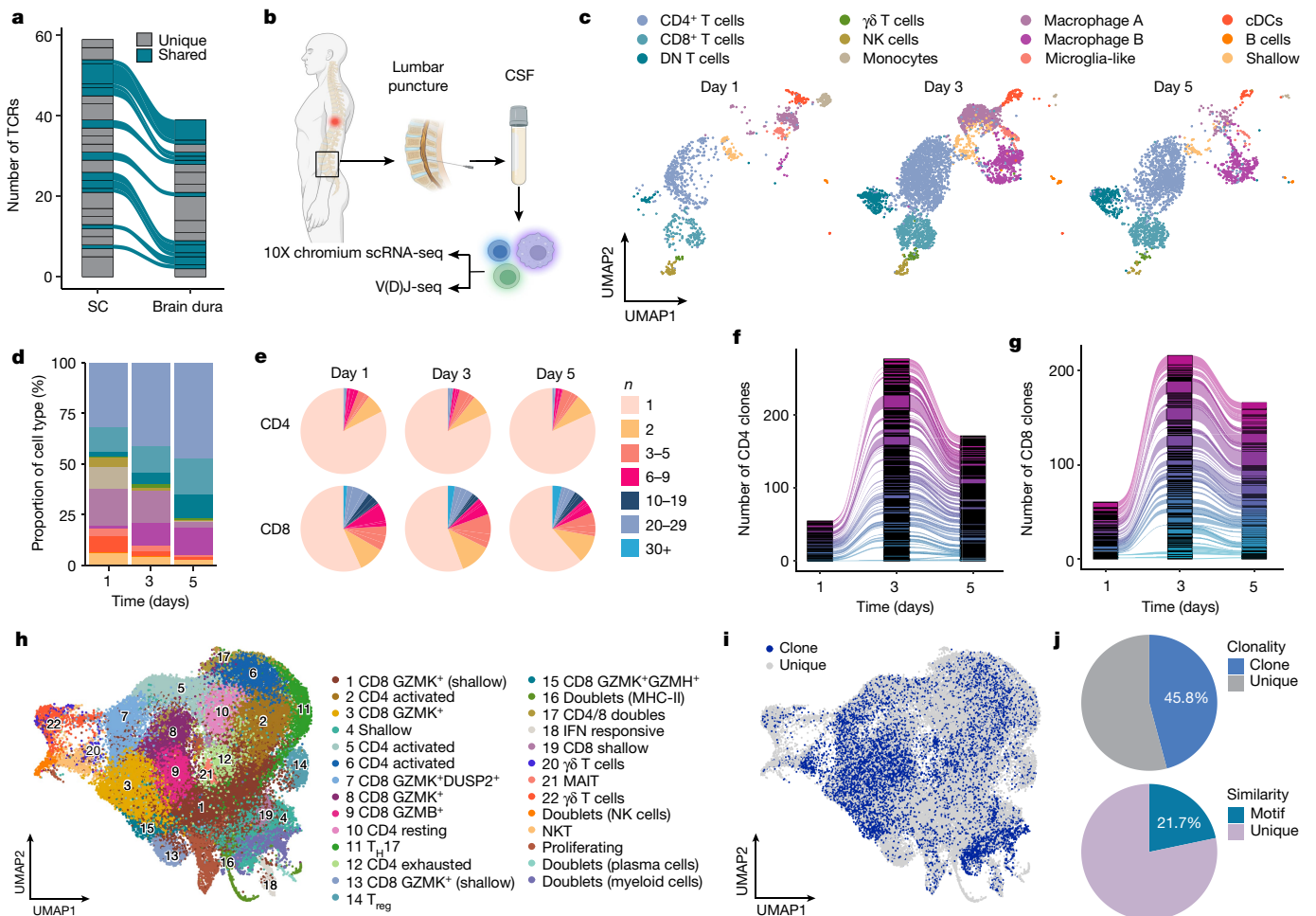


**Fig. 5 | Clonality of human CSF-derived T cells from patients with SCI.**

**a**, Alluvial plot showing shared TCRs between injured spinal cord and brain dura of mice with SCI. **b**, Schematic representation of the isolation and scRNA-seq analysis of cells from the CSF of a male patient with complete thoracic SCI. The diagram was created using BioRender (<https://biorender.com>). **c**, UMAP visualizations of scRNA-seq analysis of total cells in a human CSF sampled at different timepoints post-thoracic SCI, colour-coded by cell type. DN, double negative; NK, natural killer. **d**, Bar graph showing the proportions of each cell type at different timepoints post-thoracic SCI. **e**, Pie graphs showing the proportions of CD4<sup>+</sup> and CD8<sup>+</sup> T cell clones in human CSF samples at different

timepoints post-SCI. **f, g**, Alluvial plots showing shared CD4<sup>+</sup> (**f**) or CD8<sup>+</sup> (**g**) TCR clones in a human CSF sample at different timepoints post-SCI. **h**, UMAP visualization of scRNA-seq analysis of T cells in human CSF combined from five patients with SCI. GZMK, granzyme K; MAIT, mucosal-associated invariant T cells; T<sub>reg</sub>, regulatory T cells. **i**, UMAP visualization of T cell clonality. Cells with shared sequences of the CDR3 region of both the TCR $\alpha$  chain and the TCR $\beta$  chain are defined as a TCR clone. **j**, Pie graphs showing the proportion of T cells with clonality among total T cells (above) and the proportion of TCRs sharing motif similarity of TCR $\beta$  in T cells with clonality (below).

decreased with increasing time between injury and T cell injection (Extended Data Fig. 8g). As we did not observe harmful effects from any of the injury-associated CD4<sup>+</sup> T cell clones in the ONI model, and most of these clones exhibited neuroprotective properties with an mRNA-based TCR expression strategy in the SCI model, we considered using a therapeutic T cell cocktail to treat mice with SCI. By treating mice with SCI with T cell cocktails expressing injury-associated spinal cord CD4<sup>+</sup> TCRs (Cp, Du and Eo), we observed improved recovery compared with untreated mice (Fig. 4g).

To make a human-relevant ETA T cell prototype, we utilized CRISPR-Cas9 to remove the expression of endogenous TCRs, thereby avoiding any potential effects caused by endogenous TCRs or newly formed endogenous/reconstituted TCR pairs. We confirmed the function of guide RNAs targeting TCRs (Extended Data Fig. 8h) and subsequently transduced them into a retrovirus vector before their delivery into T cells isolated from Cas9 transgenic mice to achieve higher TCR removal efficiency (Fig. 4h). Treating mice with SCI with T cells lacking endogenous TCRs and expressing mRNA-based CRISPR-Cas9-resistant TCR<sub>Cp</sub> and TCR<sub>Du</sub> improved recovery compared with

mice treated with T cells expressing GFP as control (Fig. 4i). After treatment with T cells stably expressing TCR<sub>Cp</sub> or transiently expressing mRNA-based TCR<sub>Cp</sub>, we detected injected T cells at the injury site for as long as 4 weeks after injury in mice with SCI. This persistence may be attributed to the antigen specificity of endogenous TCRs. However, T cells in which endogenous TCRs were removed were not detectable at 4 weeks post-injection (Extended Data Fig. 8i–k). These findings indicate that the integration of CRISPR-Cas9 technology with mRNA-based protein expression yields a promising and safe avenue for T cell therapy in CNS injury.

### Clonality of human CSF T cells after SCI

After SCI in mice, shared T cell clones were observed in both the spinal cord parenchyma and brain dura (Fig. 5a and Extended Data Fig. 9a,b). These regions are anatomically segregated but are linked via their exposure to the CSF<sup>37,38</sup>, confirming the trafficking of immune cells between the CNS parenchyma and its outer meningeal layer through the CSF. Given limited access to injured spinal cord tissues from patients, we



collected CSF samples daily for 5 days from a patient in their 20s with complete (ASIA-A) thoracic SCI (T9–T10 injured) and examined the cells every other day using scRNA-seq (Fig. 5b). The major immune populations in the CSF were T cells and macrophages, with the proportion of T cells increasing over the 5 days post-injury (Fig. 5c,d and Extended Data Fig. 9c). Both CD4<sup>+</sup> and CD8<sup>+</sup> T cells displayed clonal expansion, even in the early injury phase, with many TCRs shared among different timepoints (Fig. 5e–g). We also examined immune cells in the CSF of a patient in their 70s with complete cervical SCI. Despite having more monocytes, the composition of CSF cells was similar to that of the patient with thoracic SCI (Extended Data Fig. 9d–f). Probably owing to the older age of the patient with cervical SCI, both CD4<sup>+</sup> and CD8<sup>+</sup> T cells displayed higher clonality than the patient with thoracic SCI (Extended Data Fig. 9g–i).

We further analysed gene expression and TCR similarity of T cells combined from CSF samples of five patients with SCI. Despite some T cells showing shallower gene expression, most of the CD8<sup>+</sup> T cells were present in clusters with high granzyme expression, indicating an effector or effector memory phenotype, whereas the CD4<sup>+</sup> T cell clones displayed greater diversity, including resting, activated and regulatory T phenotypes, consistent with what was observed in mice (Fig. 5h and Extended Data Fig. 10a–c). Nearly half of the T cells exhibited clonality, among which, using GLIPH analysis<sup>39</sup>, 21.7% of these T cell clones shared similarity with a common motif in the CDR3 region of TCRβ among or between individual patients (Fig. 5i,j, Extended Data Fig. 10e,f and Supplementary Table 4). These results further highlight the necessity for developing a platform for rapid TCR antigen specificity testing to facilitate the translation of these findings into human therapeutic applications.

## Discussion

In this study, we utilized scRNA-seq of T cells found within the SCI site. By reconstituting injury-associated TCRs into primary CD4<sup>+</sup> T cells, we confirmed their neuroprotective capacity in two different injury models in mice: ONI and SCI. Moreover, treatment of mice with SCI with T cells carrying self-reactive TCRs limited the inflammatory phenotype of local immune cells, lessening secondary neuronal degeneration and contributing to improved recovery. Using an mRNA-based transient TCR expression strategy, we harnessed the power of ETA T cell therapy while mitigating its autoreactive potential.

Many of the identified injury-associated CD4<sup>+</sup> T cell clones displayed antigen specificity towards MOG<sub>35–55</sub>, a well-described immunogenic peptide, albeit not as efficiently responding when compared with TCR<sub>2D2</sub> T cells. This weaker activation is to be expected, as TCR<sub>2D2</sub> T cells were isolated by screening for MOG reactivity post-immunization with adjuvant, which contrasts the derivation of endogenously recruited MOG-specific T cells following CNS injury. Other injury-associated TCRs exhibited reactivity towards neuronal peptides, although the specific antigen currently remains unidentified. Despite the benefits offered by our initial prototype of ETA T cell therapy in minimizing the detriments induced by possible self-reactivity, identifying targeting antigens is of paramount importance for developing these findings into an effective therapy. When the target antigens among different patients become identified, a CAR-T cell-like therapy could also be developed. Such an approach would not only save time on TCR sequencing and bypass the limitations of human HLA heterogeneity but also enable the generation of a ‘ready-to-use’ T cell therapy for patients with CNS injury.

Therapeutic T cells demonstrated neuroprotective efficacy primarily by modulating local inflammatory responses through the regulation of myeloid cells via IFNγ. Previous works have suggested that infiltrating monocytes are capable of mediating neuroprotection<sup>21</sup>, and IFNγ has a crucial role in the process of monocyte recruitment<sup>40</sup>. Whether ETA T cell-derived IFNγ is involved in both recruitment and phenotype

switch of the myeloid compartment at the site of injury requires further investigation. Finally, molecules such as IL-4, IL-33 and IL-10 have been demonstrated to have a role in mediating a neuroprotective effect after CNS injury<sup>21,41,42</sup>. How these molecules interact with T cell-derived IFNγ and their combined contribution to neuronal survival remains an exciting area to explore.

In summary, we generated a TCR-based, self-reactive CD4<sup>+</sup> T cell therapy for CNS injury and used mRNA-based transient TCR expression to minimize any potential autoimmune side effects. This strategy represents the first attempt at utilizing a CD4<sup>+</sup> T cell therapy to treat CNS injury and highlights the robust potential of this approach in mice. Furthermore, it identifies future research directions necessary for clinical translation to human SCI.

## Online content

Any methods, additional references, Nature Portfolio reporting summaries, source data, extended data, supplementary information, acknowledgements, peer review information; details of author contributions and competing interests; and statements of data and code availability are available at <https://doi.org/10.1038/s41586-024-07906-y>.

- GBD 2016 Traumatic Brain Injury and Spinal Cord Injury Collaborators. Global, regional, and national burden of traumatic brain injury and spinal cord injury, 1990–2016: a systematic analysis for the Global Burden of Disease Study 2016. *Lancet Neurol.* **18**, 56–87 (2019).
- Daglas, M. et al. Activated CD8<sup>+</sup> T cells cause long-term neurological impairment after traumatic brain injury in mice. *Cell Rep.* **29**, 1178–1191.e6 (2019).
- Moalem, G. et al. Autoimmune T cells protect neurons from secondary degeneration after central nervous system axotomy. *Nat. Med.* **5**, 49–55 (1999).
- Kipnis, J., Mizrahi, T., Yoles, E., Ben-Nun, A. & Schwartz, M. Myelin specific Th1 cells are necessary for post-traumatic protective autoimmunity. *J. Neuroimmunol.* **130**, 78–85 (2002).
- Miller, S. D., Karpus, W. J. & Davidson, T. S. Experimental autoimmune encephalomyelitis in the mouse. *Curr. Protoc. Immunol.* **88**, 15.11–15.120 (2010).
- Jager, A., Dardalhon, V., Sobel, R. A., Bettelli, E. & Kuchroo, V. K. Th1, Th17, and Th9 effector cells induce experimental autoimmune encephalomyelitis with different pathological phenotypes. *J. Immunol.* **183**, 7169–7177 (2009).
- Wei, S. C., Duffy, C. R. & Allison, J. P. Fundamental mechanisms of immune checkpoint blockade therapy. *Cancer Discov.* **8**, 1069–1086 (2018).
- June, C. H., O’Connor, R. S., Kawalekar, O. U., Ghassemi, S. & Milone, M. C. CAR T cell immunotherapy for human cancer. *Science* **359**, 1361–1365 (2018).
- Goverman, J. Autoimmune T cell responses in the central nervous system. *Nat. Rev. Immunol.* **9**, 393–407 (2009).
- Bradbury, E. J. & Burnside, E. R. Moving beyond the glial scar for spinal cord repair. *Nat. Commun.* **10**, 3879 (2019).
- Cohen, M. et al. Meningeal lymphoid structures are activated under acute and chronic spinal cord pathologies. *Life Sci. Alliance* **4**, e202000907 (2021).
- Crosby, C. M. & Kronenberg, M. Tissue-specific functions of invariant natural killer T cells. *Nat. Rev. Immunol.* **18**, 559–574 (2018).
- Klein, L., Klugmann, M., Nave, K. A., Tuohy, V. K. & Kyewski, B. Shaping of the autoreactive T-cell repertoire by a splice variant of self protein expressed in thymic epithelial cells. *Nat. Med.* **6**, 56–61 (2000).
- Harrington, C. J. et al. Differential tolerance is induced in T cells recognizing distinct epitopes of myelin basic protein. *Immunity* **8**, 571–580 (1998).
- Miyauchi, E. et al. Gut microorganisms act together to exacerbate inflammation in spinal cords. *Nature* **585**, 102–106 (2020).
- ELTanbouly, M. A. & Noelle, R. J. Rethinking peripheral T cell tolerance: checkpoints across a T cell’s journey. *Nat. Rev. Immunol.* **21**, 257–267 (2021).
- Holst, J. et al. Generation of T-cell receptor retrogenic mice. *Nat. Protoc.* **1**, 406–417 (2006).
- Basso, D. M. et al. Basso Mouse Scale for locomotion detects differences in recovery after spinal cord injury in five common mouse strains. *J. Neurotrauma* **23**, 635–659 (2006).
- Andreatta, M. et al. A CD4<sup>+</sup> T cell reference map delineates subtype-specific adaptation during acute and chronic viral infections. *eLife* **11**, e76339 (2022).
- Andreatta, M. et al. Interpretation of T cell states from single-cell transcriptomics data using reference atlases. *Nat. Commun.* **12**, 2965 (2021).
- Shechter, R. et al. Infiltrating blood-derived macrophages are vital cells playing an anti-inflammatory role in recovery from spinal cord injury in mice. *PLoS Med.* **6**, e1000113 (2009).
- Muhl, H. & Pfeilschifter, J. Anti-inflammatory properties of pro-inflammatory interferon-γ. *Int. Immunopharmacol.* **3**, 1247–1255 (2003).
- Sosa, R. A., Murphey, C., Robinson, R. R. & Forsthuber, T. G. IFN-γ ameliorates autoimmune encephalomyelitis by limiting myelin lipid peroxidation. *Proc. Natl Acad. Sci. USA* **112**, E5038–E5047 (2015).
- Miller, N. M., Wang, J., Tan, Y. & Dittel, B. N. Anti-inflammatory mechanisms of IFN-γ studied in experimental autoimmune encephalomyelitis reveal neutrophils as a potential target in multiple sclerosis. *Front. Neurosci.* **9**, 287 (2015).

25. Butovsky, O. et al. Microglia activated by IL-4 or IFN- $\gamma$  differentially induce neurogenesis and oligodendrogenesis from adult stem/progenitor cells. *Mol. Cell. Neurosci.* **31**, 149–160 (2006).
26. Butovsky, O. et al. Induction and blockage of oligodendrogenesis by differently activated microglia in an animal model of multiple sclerosis. *J. Clin. Invest.* **116**, 905–915 (2006).
27. Shaked, I. et al. Protective autoimmunity: interferon- $\gamma$  enables microglia to remove glutamate without evoking inflammatory mediators. *J. Neurochem.* **92**, 997–1009 (2005).
28. Mojic, M., Takeda, K. & Hayakawa, Y. The dark side of IFN- $\gamma$ : its role in promoting cancer immunoevasion. *Int. J. Mol. Sci.* **19**, 89 (2017).
29. Zhao, H. et al. Inflammation and tumor progression: signaling pathways and targeted intervention. *Signal Transduct. Target. Ther.* **6**, 263 (2021).
30. Jing, Z. L. et al. Interferon- $\gamma$  in the tumor microenvironment promotes the expression of B7H4 in colorectal cancer cells, thereby inhibiting cytotoxic T cells. *Sci. Rep.* **14**, 6053 (2024).
31. Dorrier, C. E. et al. CNS fibroblasts form a fibrotic scar in response to immune cell infiltration. *Nat. Neurosci.* **24**, 234–244 (2021).
32. Ise, W. et al. CTLA-4 suppresses the pathogenicity of self antigen-specific T cells by cell-intrinsic and cell-extrinsic mechanisms. *Nat. Immunol.* **11**, 129–135 (2010).
33. Xu, M. et al. c-MAF-dependent regulatory T cells mediate immunological tolerance to a gut pathobiont. *Nature* **554**, 373–377 (2018).
34. Petersen, T. R. et al. Characterization of MHC- and TCR-binding residues of the myelin oligodendrocyte glycoprotein 38–51 peptide. *Eur. J. Immunol.* **34**, 165–173 (2004).
35. Wan, X. et al. Pancreatic islets communicate with lymphoid tissues via exocytosis of insulin peptides. *Nature* **560**, 107–111 (2018).
36. Kacen, A. et al. Post-translational modifications reshape the antigenic landscape of the MHC I immunopeptidome in tumors. *Nat. Biotechnol.* **41**, 239–251 (2023).
37. Poulos, F. E. et al. Cerebrospinal fluid can exit into the skull bone marrow and instruct cranial hematopoiesis in mice with bacterial meningitis. *Nat. Neurosci.* **25**, 567–576 (2022).
38. Rustenhoven, J. et al. Functional characterization of the dural sinuses as a neuroimmune interface. *Cell* **184**, 1000–1016.e27 (2021).
39. Glanville, J. et al. Identifying specificity groups in the T cell receptor repertoire. *Nature* **547**, 94–98 (2017).
40. Kunis, G. et al. IFN- $\gamma$ -dependent activation of the brain's choroid plexus for CNS immune surveillance and repair. *Brain* **136**, 3427–3440 (2013).
41. Gadani, S. P., Walsh, J. T., Smirnov, I., Zheng, J. & Kipnis, J. The glia-derived alarmin IL-33 orchestrates the immune response and promotes recovery following CNS injury. *Neuron* **85**, 703–709 (2015).
42. Lima, R. et al. Systemic interleukin-4 administration after spinal cord injury modulates inflammation and promotes neuroprotection. *Pharmaceuticals* **10**, 83 (2017).

**Publisher's note** Springer Nature remains neutral with regard to jurisdictional claims in published maps and institutional affiliations.

Springer Nature or its licensor (e.g. a society or other partner) holds exclusive rights to this article under a publishing agreement with the author(s) or other rightsholder(s); author self-archiving of the accepted manuscript version of this article is solely governed by the terms of such publishing agreement and applicable law.

© The Author(s), under exclusive licence to Springer Nature Limited 2024

## Methods

### Mice

WT C57BL/6J mice (JAX: 000664) were purchased from the Jackson Laboratory and were kept in-house for at least 1 week before the start of an experiment. OT-II TCR transgenic mice (JAX: 004194), 2D2 TCR transgenic mice (JAX: 006912), MHC-II KO mice (JAX: 003584), *Irfng*<sup>-/-</sup> mice (JAX: 002287), Thy1.1 mice (JAX: 000406) and Rosa26-Cas9 mice (JAX: 026179) were purchased from the Jackson Laboratory and bred in-house. All mice were housed and bred in a temperature-controlled (22 °C) and humidity-controlled (33–39%) environment under a 12–12 h light–dark cycle and were provided with food and water ad libitum. No more than five mice were housed together per cage. All experiments were approved by the Institutional Animal Care and Use Committee of the Washington University in St. Louis. Experiments were only performed in institutions for which experimental approval was granted.

### Plasmids, antibodies and reagents

cDNA for the OT-II TCR was obtained from Addgene (52112) and cDNAs for all other TCRs were synthesized by Integrated DNA technologies (IDT). The pMIGII (52107), pCMV-T7 (133962) and pSpCas9nucl-mCherry-gRNA (167295) vector backbones were obtained from Addgene. Vector pMIG-CD4 was provided by D. Littman. Sequences of TCR $\alpha$  and TCR $\beta$  chains were linked with self-cleavage peptide P2A for expressing individual chains. TCR $\alpha$ -P2A-TCR $\beta$  was inserted into vector pMIG II for TCR reconstitution in primary T cells, inserted into vector pMIG-CD4 for TCR reconstitution in 58  $\alpha$   $\beta$  hybridoma or inserted into pCMV-T7 for mRNA synthesis. All plasmids were verified by DNA sequencing. Anti-CD3e (553057, BD Biosciences) and anti-CD28 (553294, BD Biosciences) were used for in vitro T cell activation. Anti-CD45 (103124, BioLegend), anti-MHC-II (107650, BioLegend), anti-CD3 (50-0032-82, eBioscience), anti-Ibal (ab5076, Abcam), anti-laminin (ab11575, Abcam), anti-GFAP (Z0334, Agilent Technologies), anti-Brn3a (411003, Synaptic system), anti-NeuN (ab190195, Abcam) and FluoroMeylin Red (F34652, Fisher Scientific) were used for immunostaining. Antibodies for imaging were diluted at 1:200. The flow cytometry antibodies CD45-FITC (11-0451-85), CD90.2-PE-Cy7 (25-0902-81), CD4-APC-eFluor780 (47-0041-82), CD8-APC-eFluor780 (47-0081-82), CD3-eFluor660 (50-0032-82), CD69-APC-eFluor780 (47-0691-82), CD8a-Alexa Fluor 532 (58-0081-80), CD45-BV750 (746947), TCR $\beta$ -BUV805 (748405), B220-APC (50-0452-82), TCR $\gamma$  $\delta$ -FITC (11-5711-82), CD8a-Alexa Fluor 700 (557959), T-bet-PE (12-5825-82), T-bet-PE-Cy7 (25-5825-82), FoxP3-PE-eFluor610 (61-5773-82) FoxP3-APC (17-5773-80) and ROR $\gamma$ t-BV650 (BDB564722) were purchased from eBioscience/Thermo Fisher. The flow cytometry antibodies CD11b-PE-Cy7 (552850), CD45-APC (559864), CD4-PE (553049), B220-PE (553090), V $\beta$ 5-PE (553190), CD4-PE-Cy7 (552775), CD11c-PE-Cy7 (558079) and CD4-BUV395 (563790) were purchased from BD Biosciences. Flow cytometry antibodies TCR $\beta$ -PerCP/Cy5.5 (109228), CD45-BV510 (103137), CD45-PE (103106), CD11b-PerCP/Cy5.5 (101228), CD3-Alexa Fluor 594 (100240), TCR $\beta$ -BV421 (109230), TCR $\beta$ -FITC (109206), MHC-II-BV650 (107641), Thy1.2-BV510 (105335), Thy1.1-PE (202524), V $\beta$ 11-FITC (125905), CD62L-BV785 (104440), TCR $\beta$ -BV510 (109233), CD69-PE (104508), CD44-PerCP/Cy5.5 (103032), Gata3-BV421 (653813), Gata3-APC (653806), IFN $\gamma$ -BV711 (505836), Zombie Aqua (423102) and Zombie NIR Fixable Viability Kit (423105) were purchased from BioLegend. Zombie dye and antibodies for Thy1 were diluted at 1:500. Other antibodies were diluted at 1:300.

OVA<sub>323–339</sub> peptide (O1641) was purchased from Sigma-Aldrich. MOG<sub>35–55</sub> peptide (CSO681) was purchased from CSBio. Other peptides were synthesized by GenScript.

### Cell culture and TCR reconstitution

Phoenix-ECO retroviral packaging cells (CRL-3214) were obtained from the American Type Culture Collection. The 58  $\alpha$   $\beta$  hybridoma was generated by K. Murphy and provided by D. Littman. Phoenix-ECO

cells were grown in Dulbecco's modified Eagle's medium (DMEM) with 10% (vol/vol) fetal bovine serum (FBS) and 2 mM L-glutamine. The 58  $\alpha$   $\beta$  hybridoma cells were grown in Iscove's modified Dulbecco's medium (IMDM) with 5% (vol/vol) FBS, 2 mM L-glutamine and 50  $\mu$ M  $\beta$ -mercaptoethanol. Mouse primary T cells were cultured in Roswell Park Memorial Institute (RPMI) 1640 medium supplied with 10% (vol/vol) FBS, 2 mM L-glutamine, 50  $\mu$ M  $\beta$ -mercaptoethanol, 10 mM HEPES, 1 mM sodium pyruvate, MEM non-essential amino acid and penicillin–streptomycin. Mouse primary neurons were cultured in neurobasal medium supplied with 1  $\times$  B-27, 2 mM L-glutamine and penicillin–streptomycin. All cells were grown at 37 °C in a 5% CO<sub>2</sub> incubator.

### Retrovirus preparation

Phoenix-ECO cells were seeded in six-well plates 4–8 h before transfection. Retroviral plasmids with the desired TCR genes were transfected into Phoenix-ECO cells using the TransIT-293 transfection reagent (MIR2700, Mirus Bio) as per the manufacturer's instructions. At 8–12 h after transfection, the medium was removed and replaced with IMDM with 15% (vol/vol) FBS. The supernatant containing retroviral particles were collected 48 h after transfection, filtered with a 0.45- $\mu$ m syringe filter and was then ready for infection.

### TCR reconstitution in primary T cells

Twelve-well plates were coated with anti-CD3 and anti-CD28 antibodies diluted in PBS (Ab\_CD3 of 1.5  $\mu$ g ml<sup>-1</sup>; Ab\_CD28 of 0.5  $\mu$ g ml<sup>-1</sup>) at 4 °C overnight. Spleen and lymph nodes from C57BL/6J mice were harvested, and primary CD4<sup>+</sup> T cells were isolated using the EasySep mouse CD4<sup>+</sup> T cell isolation kit (19852, STEMCELL Technologies). Isolated CD4<sup>+</sup> T cells were resuspended in culture medium containing 1  $\mu$ g ml<sup>-1</sup> Ab\_CD28, seeded in a 12-well plate, and were incubated at 37 °C. After 24 h, 1 ml of medium containing retroviral particles was added, and transfection reagent polybrene (TR-1003-G, Sigma-Aldrich) was added at a final concentration of 8  $\mu$ g ml<sup>-1</sup>. The cell and virus mixture were centrifuged at 2,000g (Eppendorf centrifuge 5910R) at 32 °C for 1 h and then incubated at 37 °C for 6–8 h. After two rounds of infection, cells were washed and resuspended in fresh medium containing 2 ng ml<sup>-1</sup> recombinant murine IL-2 (212-12, PeproTech) and transferred to a new 12-well plate. Cells were cultured at 37 °C for at least 12 h, washed and resuspend in PBS, and filtered through a 70- $\mu$ m cell strainer in preparation for injection into mice. Between 1 and 2 million functional TCR-expressing cells (2–5 million total cells) were injected intravenously into each mouse after injury. The infection efficiency was assessed by quantifying GFP-positive cells via flow cytometry.

### TCR reconstitution in 58 $\alpha$ $\beta$ hybridoma

One million hybridoma cells were resuspended in 500  $\mu$ l culture medium, mixed with 1 ml of medium containing retroviral particles, and added to a single well of a 12-well plate. The transfection reagent polybrene was added to the well at a final concentration of 5  $\mu$ g ml<sup>-1</sup>. Cells and virus mixture were centrifuged at 2,000g at 32 °C for 40 min and then incubated at 37 °C for 6 h. After infection, cells were washed and cultured in fresh medium for another 48 h. CD3<sup>+</sup>CD4<sup>+</sup> double-positive cells were isolated using fluorescence-activated cell sorting (BD Biosciences FACSAria II or BD Influx cell sorter).

### mRNA-based transient TCR expression

Sequences of TCR $\alpha$  and TCR $\beta$  chains were linked with the P2A self-cleavage peptide sequence and inserted into a pCMV-T7 vector as template for mRNA synthesis. mRNA was synthesized using the HiScribe T7 ARCA mRNA Kit (E2060, New England Biolabs) as per the manufacturer's instructions. In brief, pCMV-T7-TCR plasmid was mixed with T7 RNA polymerase and incubated at 37 °C for 45 min for RNA synthesis. DNase I was added and incubated at 37 °C for 15 min to digest DNA template. After digestion, poly(A) polymerase was used to add a poly(A)



tail by incubating at 37 °C for 40 min. Synthesized mRNA was purified with the Monarch RNA Cleanup Kit (T2050, New England BioLabs) and eluted with water. Concentration of mRNA was quantified (NanoDrop 2000, Thermo Scientific), and mRNA was analysed by agarose gel electrophoresis and then stored at -80 °C.

Primary CD4<sup>+</sup> T cells were isolated and activated with Ab\_CD3 and CD28 as previously described. Following a 24-h activation, cells were washed and resuspended in fresh medium containing 2 ng ml<sup>-1</sup> recombinant murine IL-2, transferred to a new six-well plate and incubated at 37 °C for another 12–24 h before electroporation. The 4D-Nucleofector (Lonza) and the Lonza P3 Primary Cell 4D-Nucleofector X Kit (V4XP-3024, Lonza) were used for T cell electroporation with the program DN-100. T cells were washed with PBS and resuspended in Nucleofector solution with supplement. For one reaction, 1 × 10<sup>7</sup> T cells were resuspended in 100 µl buffer with 10 µg mRNA. After electroporation, T cells were cultured in serum-free medium at 37 °C for 30 min and were then transferred to culture medium containing 2 ng ml<sup>-1</sup> recombinant murine IL-2. Cells were cultured for at least 3 h, washed, resuspended in PBS and filtered through a 70-µm cell strainer in preparation for injection into mice. Between 1 and 3 million total cells were injected intravenously into each mouse after injury.

### CRISPR-Cas9-based endogenous TCR removal

The following guide RNA (gRNA) sequences were used to target endogenous TCRs: ATTGATTTGGGAGTCAAAGT (gTCRα) and CTGACC ACGTGGAGCTGAGC (gTCRβ). DNA fragment containing the original gRNAs in the pSpCas9nucl-mCherry-gRNA plasmid was replaced with gRNAs targeting TCRs. Plasmid pSpCas9nucl-mCherry-gTCRs was electroporated into primary T cells, and TCR expression was tested by flow cytometry 2 days after electroporation. DNA fragment containing functional gRNAs targeting TCRs was then inserted into the pMIG II vector and transduced into T cells isolated from Rosa26-Cas9 mice. TCR expression was tested by flow cytometry 3 days after infection. CRISPR-Cas9-resistant TCR genes, with synonymous mutation in the gRNA-targeting region, were cloned into the pCMV-T7 vector for in vitro RNA synthesis, as described.

### Primary neuron culturing

The brain of embryonic day 15 (E15)–E19 embryo of C57BL/6J mice were used for primary neuron culturing. The skin and skull were gently removed with autoclaved forceps and the brain was carefully transferred to a dish with precooled Hank's balanced salt solution (HBSS). Leptomeninges and the choroid plexus were carefully removed from the brain and then the cortex and hippocampus were gently dissected for the following neuron culturing. The hippocampus and chopped cortex were transferred to tubes containing digestion buffer (HBSS with 20 U ml<sup>-1</sup> papain, 20 µg ml<sup>-1</sup> DNase I and 0.01% BSA) and digested at 37 °C for 20 min. Digested tissue was transferred to DMEM medium containing 10% FBS to stop digestion and gently triturated until cells were fully resuspended. Resuspended cells were filtered through 70-µm cell strainer and counted by CellDrop FL Fluorescence Cell Counter (DeNovix), then seeded to poly-L-lysine-coated 100 mm cell culture dish (5 million cells per dish) with DMEM medium containing 10% FBS. Four hours after seeding, DMEM medium was removed and replaced with prewarmed neuron culture medium (neurobasal medium with 1× B-27, L-glutamine and penicillin-streptomycin). Three days after neuron culturing, half of culture medium was replaced with fresh culture medium. Five to seven days after culturing, primary neurons were collected with cell scratch and washed with PBS. Cell pellets were weighted and resuspended with RPMI medium. Suspended cells were dounced, then lysed with ultrasonics and ready for co-culturing.

### Co-culture

**Hybridoma and antigen screening.** Splenocytes were prepared as described in 'Single-cell isolations' below. Splenic dendritic cells were

isolated with CD11c Microbeads UltraPure (130-108-338, Miltenyi Biotec) and MACS LS columns (Miltenyi Biotec) as per the manufacturer's instructions. To individual wells in a 96-well plate, 2.5 × 10<sup>5</sup> APCs were seeded and co-cultured with 5 × 10<sup>4</sup> hybridoma cells. After 20–24 h of co-culturing, the supernatant was collected for an IL-2 ELISA and cells were stained and checked by flow cytometry for GFP expression.

**Primary T cell proliferation.** Primary CD4<sup>+</sup> T cells with reconstituted TCR expression were used. For retrovirus-based TCR expression, after infection, activated T cells were transferred to a new plate with fresh culture medium containing IL-2 (2 ng ml<sup>-1</sup>) to rest for 2 days before co-culture. For mRNA-based TCR expression, T cells were rested in IL-2-containing culture medium for 6 h after electroporation and were ready for co-culture. Before co-culture, T cells were labelled with the CellTracer Violet Cell Proliferation Kit (C34557, Thermo Fisher Scientific) as per the manufacturer's instructions. Splenic dendritic cells were isolated as previously described and used as APCs. In individual wells of a 96-well plate, 5 × 10<sup>4</sup> APCs were cultured with 5 × 10<sup>4</sup> primary T cells and peptide was added to the system at a final concentration of 2 µM. Cells were co-cultured for 3 days and then stained and checked by flow cytometry.

### ELISA

Mouse IL-2 ELISA Kit (RAB0287, Sigma-Aldrich) was used as per the manufacturer's instructions to measure the concentration of IL-2 secreted by hybridomas. In brief, 20–24 h after co-culturing, supernatant was collected, diluted with the same volume of ELISA/ELISPOT Diluent, and 100 µl of sample was added to wells in an antibody-coated 96-well plate and incubated for 2 h at room temperature. Reconstituted IL-2 standard was used to generate a standard curve. After sample incubation, wells were incubated for 1 h with detection antibody, 30 min with avidin-horseradish peroxidase (HRP), and then 15 min with TMB. At least three rounds of washing were performed between each step. Absorbance was read at 450 nm after stop buffer was added to terminate the reaction.

### Single-cell isolations

Mice were injected with a lethal dose of Euthasol (10% vol/vol) and transcardially perfused with PBS containing 0.025% heparin. The lymph nodes and spleen were directly collected using forceps. For spinal cord isolation, the spine was cut on both sides and the spinal cord was flushed out using a PBS-filled syringe with an 18-gauge needle. The muscles were then removed, and spinal cord dura was peeled from the vertebra. The optic nerves from the eye to the optic chiasm were collected for the following research. Lymph nodes and spinal cord dura were directly digested at 37 °C for 30 min in prewarmed digestion buffer (RPMI-1640 medium supplemented with 2% FBS, 1 mg ml<sup>-1</sup> collagenase VIII and 0.5 mg ml<sup>-1</sup> of DNase I). Spinal cord was chopped using a surgical blade and digested in digestion buffer at 37 °C for 30 min, triturated with a 1-ml pipette and digested for another 15 min. For the spleen, digestion buffer was injected into the tissue parenchyma and incubated at 37 °C for 5 min. Then, the spleen was chopped with a surgical blade and digested in digestion buffer at 37 °C for 15 min. After digestion, enzymes were neutralized with RPMI with 10% FBS and tissue samples were mechanically homogenized and filtered through a 70-µm cell strainer. Cells were then centrifuged at 450g for 4 min and the supernatant was removed. For lymph nodes, the cell pellet was directly resuspended with RPMI containing 10% FBS and kept on ice until use. For the spleen, red blood cells were lysed with ammonium-chloride potassium (ACK) lysis buffer for 1 min at room temperature and neutralized with the same volume of RPMI containing 10% of FBS. Cells were then centrifuged, and cell pellets were resuspended with RPMI containing 10% FBS and kept on ice until use. For spinal cord and spinal cord dura, myelin was removed by resuspending cells with 30% Percoll or 12–15% BSA in PBS and centrifuged at 800g for 10 min with a slow

# Article

brake. After centrifugation, the upper myelin-containing layer and supernatant were removed, and the cell pellet was resuspended with RPMI containing 10% FBS.

## Flow cytometry and FACS

Single-cell suspensions were washed with PBS. The Zombie Aqua, Zombie NIR fixable Viability kit or DAPI was used to determine cell viability. Cell viability dyes were diluted in PBS and incubated with cells for 10 min at room temperature. After viability staining, Fc receptors were blocked for 5 min with the anti-CD16/CD32 antibody cocktail, and cells were incubated with antibody cocktails for 10 min at room temperature for surface staining. Antibodies were all diluted in FACS buffer (2% BSA, 1 mM EDTA and 20 mM HEPES in PBS). Cells were stimulated with Cell Stimulation Cocktail (00-4970-93, eBioscience) for 3 h at 37 °C for cytokine staining. For intracellular staining, the FoxP3/Transcription Factor Staining Buffer Set Kit (00-5523-00, eBioscience) was used as per the manufacturer's instructions. After staining, samples were filtered with a 70- $\mu$ m cell strainer and analysed using an Aurora spectral flow cytometer (Cytek) or sorted using a BD Biosciences FACS Aria II or BD Influx cell sorter. Data were analysed using FlowJo version 10.

## SCI and BMS scoring

Female mice 10–12 weeks of age were used for SCI. Before being assigned to surgery, the body weight of mice was assessed, and mice lighter than 19 g were removed. Mice were anaesthetized with a ketamine (100 mg kg<sup>-1</sup>)-xylazine (10 mg kg<sup>-1</sup>) mixture. The hair on the back was shaved and cleaned with betadine and alcohol. A 15-mm midline skin incision was performed over the T6–T13 vertebra, and the connective and muscle tissues were bluntly dissected to expose the lamina. A laminectomy was performed using rongeurs at T9 to expose the dorsal spinal cord. The vertebral column was stabilized with angled clamps attached to the T7 and T12, and a calibrated contusion injury of the spinal cord was induced at T9 by an Infinite Horizon Impactor (IH-0400 Impactor Precision Systems and Instrumentation) at a force of 75 K or 80 K dynes. After the injury, the muscles and skin were sutured separately, and mice were allowed to recover from anaesthesia on heating pads. After recovering from anaesthesia, mice were injected intrasubcutaneously with buprenorphine (0.05 mg kg<sup>-1</sup>) daily for the first 3 days. Water containing sulfamethoxazole and trimethoprim oral suspension (200 mg/40 mg l<sup>-1</sup>) was supplied. Soft food and nutra-gel diet (S5769-TRAY, Bio-Serv) were supplied daily. Bladders of all mice were manually voided twice a day during the experiments.

A modified BMS scoring was used to test locomotion of the hindlegs of mice with SCI. In brief, score 0 denoted no ankle movement; 1 indicated slight ankle movement; 2 denoted extensive ankle movement; 3 indicated plantar placing of the paw; 4 denoted occasional plantar stepping; 5 indicated frequent or consistent plantar stepping, no coordination; 6 denoted frequent or consistent plantar stepping, some coordination, paws parallel at initial contact; 7 indicated frequent or consistent plantar stepping, mostly coordinated, paws parallel at initial contact and rotated at lift off; and 8 denoted frequent or consistent plantar stepping, mostly coordinated, paws parallel at initial contact, lift off and tail up. The BMS for locomotion was performed every other day by two independent investigators, both of whom were blinded. The left and right limbs were scored individually, and the scores were averaged.

## ONI and retrograde labelling of RGCs

Mice 8–10 weeks of age were used for ONI. Mice were anaesthetized with a ketamine (100 mg kg<sup>-1</sup>)-xylazine (10 mg kg<sup>-1</sup>) mixture. The connective tissue above the sclera was incised, the venous sinus around the optic nerve was retracted to expose the optic nerve, and then the optic nerve was crushed using N5 self-closing forceps for 5 s. After injury, mice eyes were treated with neomycin and polymyxin B sulfates and bacitracin zinc ophthalmic ointment. Mice were allowed to recover from anaesthesia on heating pads and injected subcutaneously with buprenorphine

sustained release analgesia (0.5 mg kg<sup>-1</sup>) once they were fully awake. Fluoro-Gold injection was performed 3 days before ONI. Mice were anaesthetized and immobilized in a stereotactic device. The skull was exposed, and holes were drilled 2.9 mm caudal to Bregma and 0.5 mm lateral to the midline. An injection of 1  $\mu$ l of 4% Fluoro-Gold (H-22845, Invitrogen) was made 2 mm below the meningeal surface at a rate of 0.5  $\mu$ l min<sup>-1</sup> using a Hamilton syringe and an automatic injector. The dye was allowed to diffuse into the tissue for 1 min before the syringe was removed and the scalp was sutured closed. Mice were allowed to recover from anaesthesia on heating pads and injected intraperitoneally with buprenorphine sustained release analgesia (0.5 mg kg<sup>-1</sup>) once they were fully awake.

## scRNA-seq

**Mouse spinal cord TCR scRNA-seq.** Ten weeks of age female C57BL/6J mice were subjected to SCI as described in the 'SCI and BMS scoring' section. The injured portion of spinal cord (injury site of  $\pm$ 0.5 mm) was collected for T cell isolation 2 weeks after injury. Single-cell suspensions were generated as described in 'Single-cell isolations', and cell-surface staining and sorting were performed as described in 'Flow cytometry and FACS'. Viable T cells (DAPI<sup>-</sup>CD45<sup>+</sup>Thy1.2<sup>+</sup>CD4<sup>+</sup> or DAPI<sup>-</sup>CD45<sup>+</sup>Thy1.2<sup>+</sup>CD8<sup>+</sup>) were sorted into a 1.5-ml Eppendorf tube with RPMI medium containing 10% FBS. CD4<sup>+</sup> and CD8<sup>+</sup> T cells were combined. T cells were washed, counted and resuspended with PBS containing 0.04% BSA. T cell samples were loaded onto a 10X Genomics Chromium platform for gel beads-in emulsions, and the Mouse T cell Chromium Single Cell V(D)J Enrichment Kit and Chromium Single Cell 5' Library & Gel Bead Kit were used separately to generate a cDNA library targeting the TCR and for transcriptome expression. Libraries were sequenced on the Illumina NextSeq 500 using pair-ended sequencing.

Reads were aligned to the mm10 genome using the Cellranger software pipeline provided by 10X genomics. The resulting filtered gene by cell matrices of unique molecular identifier (UMI) counts were read into R using the read10xCounts function from the Droplet Utils package. Filtering was applied to remove low-quality cells by excluding cells expressing greater than 20% mitochondrial gene expression, but aggressive filtering was avoided for most comparisons because of the desire to preserve clones and emphasis on their analysis. Distribution of total reads per cell, unique features per cell and ribosomal fraction of reads were all examined per sample to ensure no outliers were the focus of the analysis. Expression values for the remaining cells were then normalized using the scran and scater packages<sup>43</sup>. The resulting log<sub>2</sub> values were transformed to the natural log scale for compatibility with the Seurat (v3) pipeline<sup>44,45</sup>.

Filtered and normalized matrices were used as input to the Seurat pipeline, and samples were then integrated with the use of FindIntegrationAnchors and IntegrateData. Expression values were scaled across each gene, the effects of sequencing depth per cell, the number of unique features and the percent mitochondrial reads were regressed out. Principal components analysis was conducted and an elbow plot was used to select components for UMAP analysis and clustering. Shared nearest neighbour (SNN) clustering optimized with the Louvain algorithm, as implemented by the Seurat FindClusters function, was performed before manual annotation of clusters based on the expression of canonical gene markers. Statistical analysis of cluster proportions was done via a permutation test with 1,000 instances followed by bootstrapping to produce a *P* value and confidence interval.

The Cellranger vDJ command was used to generate annotation files for the V(D)J receptors for each cell sequenced. The filtered contig annotation csv files were then read in to R and first filtered for productive barcodes. Then, for each comparison of interest, the .csv files were concatenated and analysed together. Barcodes with no consensus sequence were first filtered out, after verification that all had 'multi' recorded for the chain. The  $\alpha$ -chain and  $\beta$ -chain were then separated and only those cell barcodes with exactly one of each were selected for

further processing. Clones were defined as those barcodes that had the same amino acid sequence for both  $\alpha$ -chain and  $\beta$ -chain sequences. These clones were then matched with mRNA transcript expression from the processed mRNA scRNA-seq described above with the use of Seurat's GetAssayData. Clones were classified as CD4<sup>+</sup> if they expressed greater than 0 transcripts of *Cd4* and exactly 0 of *Cd8b1*, had greater than 0 transcripts of *Foxp3*, expressed greater than 0.5 transcripts of *Cd4* and less than 0.9 of *Cd8b1*, or had 0 transcripts for both genes and were clustered in a definitively *Cd4*-positive cluster; they were classified as CD8<sup>+</sup> if they expressed greater than 0 transcripts of *Cd8b1* and exactly 0 of *Cd4*, or they had 0 for both genes and greater than 0 transcripts of either *Cd8a* or *Nkg7*. Network plots were created in R with the use of the qgraph package<sup>46</sup> (v1.6.9).

**Human CSF TCR scRNA-seq.** Human CSF samples used in the scRNA-seq experiments were obtained with informed consent for research use and approved by the review board of Washington University in St. Louis under IRB# 202012050. Human CSF was collected via a lumbar drain daily from patients with SCI. Of CSF, 10 ml was used at each timepoint for cell isolation. CSF was transferred into a 15-ml centrifuge tube and centrifuged at 500g for 5 min. The supernatant was removed, and cell pellet was resuspended with PBS containing 0.04% BSA and filtered with a 40- $\mu$ m cell strainer. Cell number and viability were determined using Viastain AOP1 Staining Solution (CS2-0106, Nexcelom Bioscience) and the CellDrop FL Fluorescence Cell Counter (DeNovix). Cell samples were loaded onto a 10X Genomics Chromium platform for gel beads-in-emulsions, and the Human T cell Chromium Single Cell V(D)J Enrichment Kit and Chromium Single Cell 5' Library & Gel Bead Kit were used separately to generate a cDNA library targeting the TCR and for transcriptome expression. Libraries were sequenced on the Illumina NextSeq 500 using pair-ended sequencing.

Reads were aligned to the hg38 genome using the Cellranger software pipeline provided by 10X genomics. The resulting filtered gene by cell matrices of UMI counts were read into R using the read10xCounts function from the Droplet Utils package. To preserve clonal cells for later analysis, they were first identified and subset out. The subsequent remaining cells were analysed with the scds package<sup>47</sup> with thresholds set to remove 5% with the highest doublet score (corresponding to the expected rate of doublets with 10X sequencing), followed by manual removal of cells that had greater than 2.5 standard deviations from the mean of either total RNA count or unique features in both directions, or percent of mitochondrial transcripts above the mean. Finally, clonal cells were merged back into the dataset. Expression values for the final subset were then normalized using the scan and scater packages<sup>43</sup>. The resulting log<sub>2</sub> values were transformed to the natural log scale for compatibility with the Seurat (v3) pipeline<sup>44,45</sup>.

The filtered and normalized matrix was used as input to the Seurat pipeline and cells were scaled across each gene before the selection of the top 2,000 most highly variable genes using variance-stabilizing transformation. Principal components analysis was conducted, and an elbow plot was used to select components for UMAP analysis and clustering. SNN clustering optimized with the Louvain algorithm, as implemented by the Seurat FindClusters function, was performed before manual annotation of clusters based on expression of canonical gene markers.

The Cellranger vdj command was used to generate annotation files for the V(D)J receptors for each cell sequenced. The filtered contig annotation csv files were then read into R and first filtered for productive barcodes. Then, for each comparison of interest, the .csv files were concatenated and analysed together.  $\alpha$ -Chains and  $\beta$ -chains were then separated and only those cell barcodes with exactly one of each were selected for further processing. Clones were defined as those barcodes that had the same nucleic acid sequence for both  $\alpha$ -chain and  $\beta$ -chain sequences. These clones were then matched with mRNA transcript expression from the processed mRNA scRNA-seq described above

with the use of Seurat's GetAssayData. Clones were classified as CD4<sup>+</sup> if they expressed greater than 0 transcripts of *CD4* and exactly 0 of *CD8B*, had greater than 0 transcripts of *FOXP3*, expressed greater than 0.5 transcripts of *CD4* and less than 0.9 of *CD8B*, or had 0 transcripts for both genes and were clustered in a definitively CD4<sup>+</sup> cluster; they were classified as CD8<sup>+</sup> if they expressed greater than 0 transcripts of *CD8B* and exactly 0 of *CD4*, or they had 0 for both genes and greater than 0 transcripts of either *CD8A* or *NKG7*.

Multi-patient integrated analysis was then performed with initial quality filtering as described above for all samples to the point of normalization. Filtered and normalized matrices were used as input to the Seurat pipeline and samples were then integrated with the use of FindIntegrationAnchors and IntegrateData before resuming with analysis as described above to identify cell types. T cells were then subset out and reclustered. Motif-based analysis from clonal V(D)J sequences was performed with GLIPH2 (ref. 48). Network plots were created in R with the use of the qgraph package.

**CD45<sup>+</sup> immune cell scRNA-seq.** Female 10-week-old C57BL/6J mice were induced with SCI followed immediately by injection of Cp-T cells or PBS as control. The injured portion of the spinal cord (injury site of  $\pm 0.5$  mm) was collected for cell isolation 7 days after injury. Single-cell suspensions were generated as described in 'Single-cell isolations'. CD45 Microbeads UltraPure (130-052-301, Miltenyi Biotec) and MACS LS columns (Miltenyi Biotec) were used as per the manufacturer's instructions to isolate the CD45<sup>+</sup> population. Isolated CD45<sup>+</sup> cells were resuspended in PBS containing 0.04% BSA. Cell number and viability were determined using Viastain AOP1 Staining Solution (CS2-0106, Nexcelom Bioscience) and the CellDrop FL Fluorescence Cell Counter (DeNovix). Sample loading and library construction were performed using the 10X Genomics Chromium platform and Chromium Single Cell 3' Library & Gel Bead Kit (v3). Libraries were sequenced on the Illumina NextSeq 500 using pair-ended sequencing.

Reads were aligned to the mm10 genome using the Cellranger software pipeline provided by 10X genomics. The resulting filtered gene by cell matrices of UMI counts were read into R using the read10xCounts function from the Droplet Utils package. To preserve clonal cells for later analysis, they were first identified and subset out. The subsequent remaining cells were analysed with the scds package<sup>47</sup> with thresholds set to remove 5% with the highest doublet score (corresponding to the expected rate of doublets with 10X sequencing), followed by manual removal of cells that had greater than 2 standard deviations from the mean of either total RNA count or unique features in both directions, or percent of mitochondrial transcripts above the mean. Finally, clonal cells were merged back into the dataset. Expression values for the final subset were then normalized using the scan and scater packages<sup>43</sup>. The resulting log<sub>2</sub> values were transformed to the natural log scale for compatibility with the Seurat (v3) pipeline<sup>44,45</sup>.

The filtered and normalized matrix was used as input to the Seurat pipeline, and cells were scaled across each gene before the selection of the top 2,000 most highly variable genes using variance-stabilizing transformation. Principal components analysis was conducted, and an elbow plot was used to select components for UMAP analysis and clustering. SNN clustering optimized with the Louvain algorithm, as implemented by the Seurat FindClusters function, was performed before manual annotation of clusters based on expression of canonical gene markers. Subclustering was performed by subsetting out cell types of interest and repeating scaling, identification of highly variable genes, principal components analysis, clustering and annotation based on markers.

For analysis of differentially expressed genes between conditions, each sample was filtered to include genes that had at least 5 transcripts in at least 5 cells, then the top 2,000 highly variable genes were determined and included for further analysis using the Single-CellExperiment modelGeneVar and getTopHVGs functions. After



# Article

filtering, observational weights for each gene were calculated using the ZINB-WaVE zinbFit and zinbwave functions<sup>49</sup>. These were then included in the edgeR model, which was created with the glmFit function, by using the glmWeightedF function<sup>50</sup>. Results were then filtered using a Benjamini–Hochberg-adjusted  $P$  value threshold of less than 0.05 as statistically significant. Over-representation enrichment analysis with Fisher’s exact test was used to determine significantly enriched gene ontology terms (adjusted  $P < 0.05$ ) for the sets of significantly differentially expressed genes. For each gene set, genes were separated into upregulated and downregulated, and separately<sup>51</sup>, the enrichGO function from the clusterProfiler package was used with a gene set size set between 10 and 500 genes and the  $P$  values were adjusted using the Benjamini–Hochberg correction<sup>52</sup>.

To evaluate potential cell–cell and ligand–receptor interactions, the RNAMagnet package<sup>53</sup> was utilized, running the RNAMagnetSignaling function, and then extracted matches above a threshold of 0.01 for T cells from each condition and each other cell type in the dataset.

**T cell FACS-seq.** Female 10-week-old C57BL/6J mice were subjected to SCI as described in the ‘SCI and BMS scoring’ section. CD4<sup>+</sup> T cells with retrovirus-based TCR<sub>CP</sub> and GFP expression were injected intravenously into the mice after injury. The injured part of spinal cord (injury site of ±0.5 mm) and spleen were collected for T cell isolation 2 weeks after injury. Single-cell suspensions were generated as described in ‘Single-cell isolations’ and cell-surface staining and sorting were performed as described in ‘Flow cytometry and FACS’. Cp-T cells (DAPI<sup>+</sup> CD45<sup>+</sup> CD11b<sup>+</sup> TCRβ<sup>+</sup> CD4<sup>+</sup> CD8<sup>+</sup> GFP<sup>+</sup>) from the injured spinal cord and spleen were sorted into individual wells of a 96-well plate with 10× lysis buffer (635013, TaKaRa) and 5% RNase inhibitor (O3335399001, Millipore Sigma). Plates were sealed with an adhesive plate seal, frozen rapidly over dry ice after sorting and stored at –80 °C until use.

Library preparation was performed with 2 μl of single-cell lysates arrayed in 96-well PCR plates. ds-cDNA was prepared using a protocol adapted from the Takara-Clontech SMARTer methods and scaled to a 5 μl reaction volume. This method introduces a unique barcode upstream of the polyA tail using a modified oligo-dT primer. In brief, 0.5 μl of the Takara dilution buffer with 5% RNase inhibitor and 0.25 μl of 25 μM FACS-seq barcode primer were added to the lysate and heated to 72 °C for 3 min. Then, 2.25 μl of the reverse transcription master mix was added to each well with 1 μl 5× first strand buffer, 0.125 μl 100 mM DTT, 0.25 μl 20 mM dNTPs, 0.25 μl 50 μM FACS-seq template switch oligo (TSO) primer, 0.125 μl RNase inhibitor and 0.5 μl SMARTscribe reverse transcriptase (Takara). The reaction was incubated at 42 °C for 90 min, 70 °C for 10 min, then a 4 °C hold. All wells from the plate were then pooled and purified with Ampure XP beads (Beckman Coulter) with a 1× ratio. cDNA was eluted in 39 μl water. cDNA was amplified using 5 μl 10× PCR buffer, 2 μl 10 mM dNTPs, 2 μl 12 μM FACS-seq206 TSO PCR primer and 2 μl 50× Advantage 2 Polymerase (Takara). PCR conditions were 95 °C for 1 min, 16 cycles of 95 °C for 15 s, 65 °C for 30 s, 68 °C for 6 min, 1 cycle of 72 °C for 10 min, followed by a 4 °C hold. cDNA was purified with 1.2× Ampure bead cleanup, measured with the 209 Qubit dsDNA assay, and visualized on a bioanalyzer. cDNA was fragmented using a Covaris E220 210 sonicator using peak incident power of 18, duty factor of 20%, and cycles per burst of 50 for 120 s. cDNA was blunt ended, had an A base added to the 3’ ends and had Illumina sequencing adapters ligated to the ends. Ligated fragments were then amplified for 16 cycles using a standard Illumina i7 primer to introduce an index sequence and FACS-seq Lib PCR 1.0 specific to fragments containing the cell barcode added during cDNA synthesis. Fragments were sequenced on an Illumina NextSeq using paired-end reads with 25 cycles for read 1, 7 cycles for the i7 index, and 100 cycles for the paired read. The sequencing run was performed with a custom sequencing primer for read 1 to read the 10-bp barcode unique to each cell. The i7 index allows for multiple plates to be sequenced together. Read 2 contains the mRNA sequences. The FACS-seq barcode:

AAGCAGTGGTATCAACGCAGAGTACXXXXXXXXXXXXTTTTTTTTTTTTTTT TTTTTTTTTTTTTTTT.VN.10Xs in the FACS-seq barcode primer is a 10-nt barcode made up of unique sequences for each sample to be pooled. The FACS-seq TSO: AAGCAGTGGTATCAACGCAGAGTG-AATrGrGrG; the FACS-seq TSO PCR: AAGCAGTGGTATCAACGCAGAGT; the FACS-seq lib PCR 1.0: AATGATACGGCGACCACCGAGATCTACACGCGCTGTCCGC GGAAAGCAGTGGTATCAACGCAGAGT\*A\*C; and the FACS-seq custom read 1: GCCTGTCCGCGGAAGCAGTGGTATCAA-CGCAGAGTAC.

Sequencing was demultiplexed with a custom Python and perl script, then aligned to the Ensembl release 76 top-level assembly with STAR (v2.5.1a). Gene counts were derived from the number of uniquely aligned unambiguous reads by Subread: featureCount (v1.4.6-p5). Further analysis was performed in R. First, cells were filtered to remove any that were 3 standard deviations outside the mean for either total features or total reads. This resulted in 143 cells for further analysis. Expression values for the remaining cells were then normalized using the scran and scater packages<sup>43</sup> and transformed to the natural log scale for compatibility with the Seurat (v3) pipeline<sup>44,45</sup>. Expression values were scaled across each gene, the effects of sequencing depth per cell, the number of unique features and the percent of mitochondrial reads were regressed out. Principal components analysis was conducted, and an elbow plot was used to select components for UMAP visualization.

For analysis of differentially expressed genes between conditions, each sample was filtered to include genes that had at least 5 transcripts in at least 5 cells, then the top 2,000 highly variable genes were determined and included for further analysis using the SingleCellExperiment modelGeneVar and getTopHVGs functions. After filtering, observational weights for each gene were calculated using the ZINB-WaVE zinbFit and zinbwave functions<sup>49</sup>. These were then included in the edgeR model, which was created with the glmFit function, by using the glm-WeightedF function<sup>50</sup>. Results were then filtered using a Benjamini–Hochberg-adjusted  $P$  value threshold of less than 0.05 as statistically significant. Over-representation enrichment analysis with Fisher’s exact test was used to determine significantly enriched gene ontology terms (adjusted  $P < 0.05$ ) for the sets of significantly differentially expressed genes. For each gene set, genes were separated into upregulated and downregulated, and separately<sup>51</sup>, the enrichGO function from the clusterProfiler package was used with a gene set size set between 10 and 500 genes, and  $P$  values were adjusted using the Benjamini–Hochberg correction<sup>52</sup>. Normalized enrichment scores and  $P$  values for the gene set enrichment analysis were computed using the fgsea R package<sup>54</sup>.

## Tissue collection and processing for IHC

Mice were euthanized using a lethal dose of anaesthetics (Euthasol, 10% vol/vol) by intraperitoneal injection and transcardially perfused with PBS containing 0.025% heparin. For whole-mount optic nerve staining, the skull was removed and the optic nerve was cut at the optic chiasma. Then, optic nerves between the eye and the optic chiasma were collected and fixed with 4% paraformaldehyde (PFA) at 4 °C overnight. For whole-mount retina staining, eyes were collected, immersed in PBS and cut through the corneal limbus. The lens was removed, and the retina was carefully separated from the sclera and the choroid with a brush. Four cuts were made towards the optic disc and another cut was made to separate the retina with the optic nerve. The retina was flattened and mounted on nylon membrane filter paper and fixed with 4% PFA at 4 °C overnight. For the spinal cord, the spine was cut on both sides, and muscles were removed from the vertebral. The spinal cord together with the vertebrae were fixed with 4% PFA at 4 °C for 48 h. After fixation, the vertebrae were cut and both the bone and spinal cord dura were removed from spinal cord. The spinal cord was then transferred to PBS with 30% sucrose until fully immersed, and then embedded in optimal cutting temperature compound, frozen rapidly over dry ice and stored at –20 °C. Sagittal sections of the spinal cord (40 μm thick) were cut on a cryostat (Leica) and sections were kept in PBS with 0.25% sodium azide at 4 °C.

For immunofluorescence staining, tissues were rinsed in PBS and washed with PBS-T (0.3% Triton X-100 in PBS) twice, followed by incubation in blocking buffer (PBS-T with 1% BSA and 2% normal chicken serum) for 1 h at room temperature with gentle agitation. Samples were then incubated with primary antibodies in incubation buffer (PBS-T with 1% BSA) overnight at 4 °C, washed three times with PBS-T and incubated with secondary antibodies in PBS-T for 2 h at room temperature. Slices were washed twice with PBS-T, and nuclei were counterstained with DAPI, followed by washing with PBS. Free-floating spinal cord sections, optic nerve or paper-attached retina were then mounted on microscope slides. For Fluoro-Gold-labelled tissues, samples were washed with PBS after PFA fixation and directly mounted, ready for imaging.

### Microscopy and image analysis

Mounted tissues were stored at 4 °C for no more than 1 week until images were acquired. Sliced spinal cords and whole-mounted retina were imaged using a widefield microscope (VS200-S6, Olympus). Whole-mounted optic nerves were imaged using a confocal microscope (DMI-8 Stellaris, Leica). Quantitative analysis of acquired images was performed using the Fiji package for ImageJ. For RGC quantification, four quadrants (0.25 mm × 0.25 mm) at 1-mm distance from the centre of the retina were chosen for each retina, and the RGC counting results were averaged to generate the value of single retina. For quantification of the spinal cord scar region, every third section over the injury site was collected for GFAP staining and scar quantification. Sections covering 3 mm (centre of injury site of ±1.5 mm) of the spinal cord were analysed. The coverage of GFAP<sup>+</sup> to DAPI<sup>+</sup> area was quantified, and the result from five slides were averaged to generate the value for a single mouse.

### MHC-II peptidome and mass spectrometry

**Isolation of the MHC-II peptidome.** Single cells isolated from the spinal cord, spinal cord meninges (dura mater) and lymph nodes as described in ‘Single-cell isolations’ were lysed with lysis buffer (40 mM MEGA 8, 40 mM MEGA 9, 1 mM phenylmethylsulfonyl fluoride, 0.2 mM iodoacetamide, 20 µg ml<sup>-1</sup> leupeptin and Roche complete protease inhibitor cocktail) and agitated for 1 h at 4 °C. The resulting cell lysate was centrifuged at 20,000g for 25 min at 4 °C and the pellet was discarded. The supernatant was collected and incubated with polyclonal mouse immunoglobulin G (Bio X Cell; 1.5 mg antibody per sample) bound to Sepharose 4B at 4 °C for 45 min to remove nonspecific-binding peptides. The flow through containing peptide–MHC-II complexes was collected and added to a tube containing PBS-washed sepharose conjugated to the anti-I-A<sup>b</sup> antibody (Y-3P; 1.5 mg per sample) and incubated at 4 °C overnight. The I-A<sup>b</sup>–sepharose was applied to a column and washed four times as follows: 10 ml 150 mM NaCl and 20 mM Tris (pH 7.4); 10 ml 400 mM NaCl and 20 mM Tris (pH 7.4); 10 ml 150 mM NaCl and 20 mM Tris (pH 7.4); and 10 ml 20 mM Tris (pH 8.0). Peptides were then eluted with 10% acetic acid and dried using a SpeedVac. Eluted peptides were passed over detergent removal spin columns (Pierce) to remove traces of remaining detergent and were further cleaned using C18 Spin Columns from Thermo Fisher Scientific (Pierce).

**Mass spectrometry.** A Dionex UltiMate 3000 system (Thermo Scientific) was coupled to an Orbitrap Fusion Lumos (Thermo Scientific) through an EASYSpray ion source (Thermo Scientific). Peptide samples were reconstituted in 2% acetonitrile (ACN)/0.1% formic acid and loaded (15 µl min<sup>-1</sup> for 3 min) onto a trap column (100 µm × 2 cm, 5 µm Acclaim PepMap 100 C18 at 50 °C), eluted (200 nl min<sup>-1</sup>) onto an EASY-Spray PepMap RSLC C18 column (2 µm, 50 cm × 75 µm ID at 50 °C; Thermo Scientific) and separated with the following gradient, all percent of buffer B (0.1% formic acid in ACN): 0–110 min at 2–22%; 110–120 min at 22–35%; 120–130 min at 35–95%; 130–150 min with isocratic at 95%; 150–151 min at 95–2%, and 151–171 min with isocratic at 2%. Spray voltage was 1,900 V, ion transfer tube temperature was 275 °C and radio frequency lens was 30%. Mass spectrometry scans were acquired in profile

mode and MS/MS scans in centroid mode, for ions with charge states of 2–5, with a cycle time of 3 s. For higher-energy collisional dissociation, mass spectra were recorded from 375 to 1,500 Da at 120,000 resolution (at  $m/z = 200$ ), and MS/MS was triggered above a threshold of  $2.0 \times 10^4$ , with quadrupole isolation (0.7 Da) at 30,000 resolution and collision energy of 30%. Dynamic exclusion was used (30 s).

**Mass spectrometry data analysis.** Data files were uploaded to PEAKS Studio 10.6 (Bioinformatics Solutions) for processing, de novo sequencing and database searching. Resulting sequences were searched against the UniProt Mouse Proteome database (downloaded 4 May 2020; 22,106 entries) with mass error tolerances of 10 ppm and 0.01 Da for parent and fragment, respectively, no enzyme specificity, and oxidation (M), deamidation (NQ), pyroglutamate from Q and cysteine oxidation to cysteic acid as variable modifications. The Common Repository for Adventitious Proteins database ([www.thegpm.org/crap/](http://www.thegpm.org/crap/)) was used to identify contaminant proteins. False discovery rate estimation was enabled. Peptides were filtered for  $-10 \log P \geq 15$ , and proteins were filtered for  $-10 \log P \geq 0$  and one unique peptide matching the significance cut-off.

### Reporting summary

Further information on research design is available in the Nature Portfolio Reporting Summary linked to this article.

### Data availability

Raw data of all single-cell sequencing are available on the Gene Expression Omnibus under the accession numbers GSE216391 and GSE189812. Raw data of the mass spectrometry peptidome have been uploaded on MassIVE under the accession number MSV000091130.

- McCarthy, D. J., Campbell, K. R., Lun, A. T. & Wills, Q. F. Scater: pre-processing, quality control, normalization and visualization of single-cell RNA-seq data in R. *Bioinformatics* **33**, 1179–1186 (2017).
- Butler, A., Hoffman, P., Smibert, P., Papalexi, E. & Satija, R. Integrating single-cell transcriptomic data across different conditions, technologies, and species. *Nat. Biotechnol.* **36**, 411–420 (2018).
- Lun, A. T., McCarthy, D. J. & Marioni, J. C. A step-by-step workflow for low-level analysis of single-cell RNA-seq data with Bioconductor. *F1000Res.* **5**, 2122 (2016).
- Epskamp, S., Cramer, A. O. J., Waldorp, L. J., Schmittmann, V. D. & Borsboom, D. qgraph: Network visualizations of relationships in psychometric data. *J. Stat. Softw.* <https://doi.org/10.18637/jss.v048.i04> (2012).
- Bais, A. S. & Kostka, D. scds: Computational annotation of doublets in single-cell RNA sequencing data. *Bioinformatics* **36**, 1150–1158 (2020).
- Huang, H., Wang, C., Rubelt, F., Scriba, T. J. & Davis, M. M. Analyzing the *Mycobacterium tuberculosis* immune response by T-cell receptor clustering with GLIPH2 and genome-wide antigen screening. *Nat. Biotechnol.* **38**, 1194–1202 (2020).
- Van den Berge, K. et al. Observation weights unlock bulk RNA-seq tools for zero inflation and single-cell applications. *Genome Biol.* **19**, 24 (2018).
- Robinson, M. D., McCarthy, D. J. & Smyth, G. K. edgeR: a Bioconductor package for differential expression analysis of digital gene expression data. *Bioinformatics* **26**, 139–140 (2010).
- Hong, G., Zhang, W., Li, H., Shen, X. & Guo, Z. Separate enrichment analysis of pathways for up- and downregulated genes. *J. R. Soc. Interface* **11**, 20130950 (2014).
- Yu, G., Wang, L. G., Han, Y. & He, Q. YclusterProfiler: an R package for comparing biological themes among gene clusters. *OMICS* **16**, 284–287 (2012).
- Baccin, C. et al. Combined single-cell and spatial transcriptomics reveal the molecular, cellular and spatial bone marrow niche organization. *Nat. Cell Biol.* **22**, 38–48 (2020).
- Korotkevich, G. et al. Fast gene set enrichment analysis. Preprint at *bioRxiv* <https://doi.org/10.1101/060012> (2021).

**Acknowledgements** We thank S. Smith and D. Gibson for editing the manuscript; all the members of the Kipnis laboratory for helpful discussion of the results presented here; the Flow Cytometry, Fluorescence Activated Cell Sorting Core, McDonnell Genome Institute (MGI), Animal behavior core, and the Center for Cellular Imaging (WUCI) of Washington University in St. Louis; D. Littman and C. Hsieh for their advice on the TCR–antigen screening system; and C. Crewe for sharing equipment.

**Author contributions** W.G. conceived the study, designed and performed the experiments, analysed the data, prepared the figures and wrote the original draft of the manuscript. M.W.K. contributed to the MHC-II peptidome analysis and helped with antigen screening. T.D. performed all the scRNA-seq analyses. I.S. helped with all surgeries and helped assess post-injury mouse locomotion. C.F.L. performed liquid chromatography–mass spectrometry and raw data analysis. P.B. provided intellectual contribution and helped with FACS-seq

# Article

---

analysis. J.R. provided intellectual contribution, helped with FACS-seq experiments and helped edit the manuscript. S.D. and X.G. helped with human CSF cell sequencing. M.A.R.-C., W.Z.R. and C.M. provided human CSF samples. T.W.S. and Y.M. performed the protein modification analysis of the MHC-II-binding peptidome. J.K. conceived the study, directed the research, provided funding and edited the manuscript.

**Competing interests** W.G., M.W.K., P.B. and J.K. hold provisional patent applications related to findings presented here.

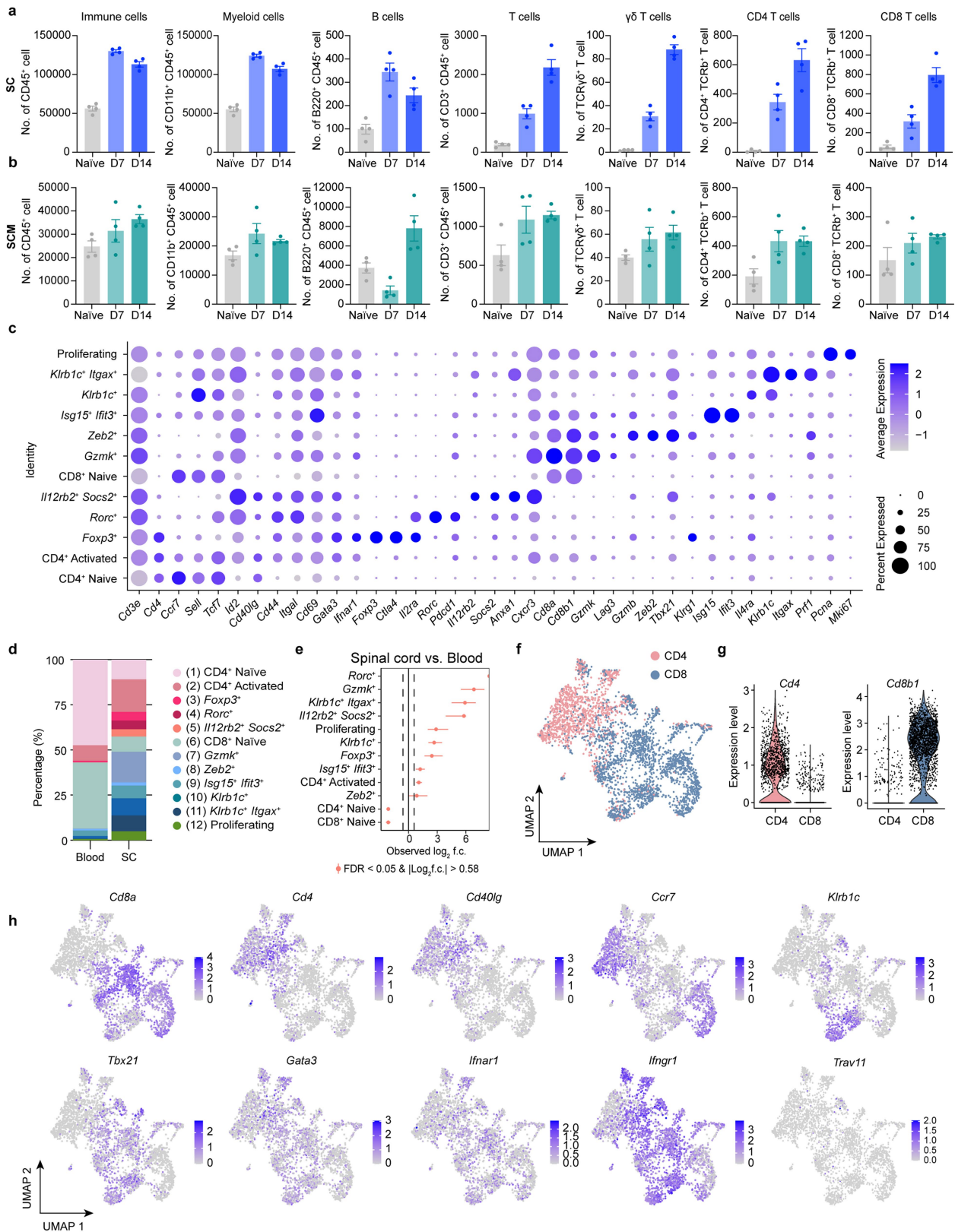
## **Additional information**

**Supplementary information** The online version contains supplementary material available at <https://doi.org/10.1038/s41586-024-07906-y>.

**Correspondence and requests for materials** should be addressed to Wenqing Gao or Jonathan Kipnis.

**Peer review information** *Nature* thanks the anonymous reviewers for their contribution to the peer review of this work.

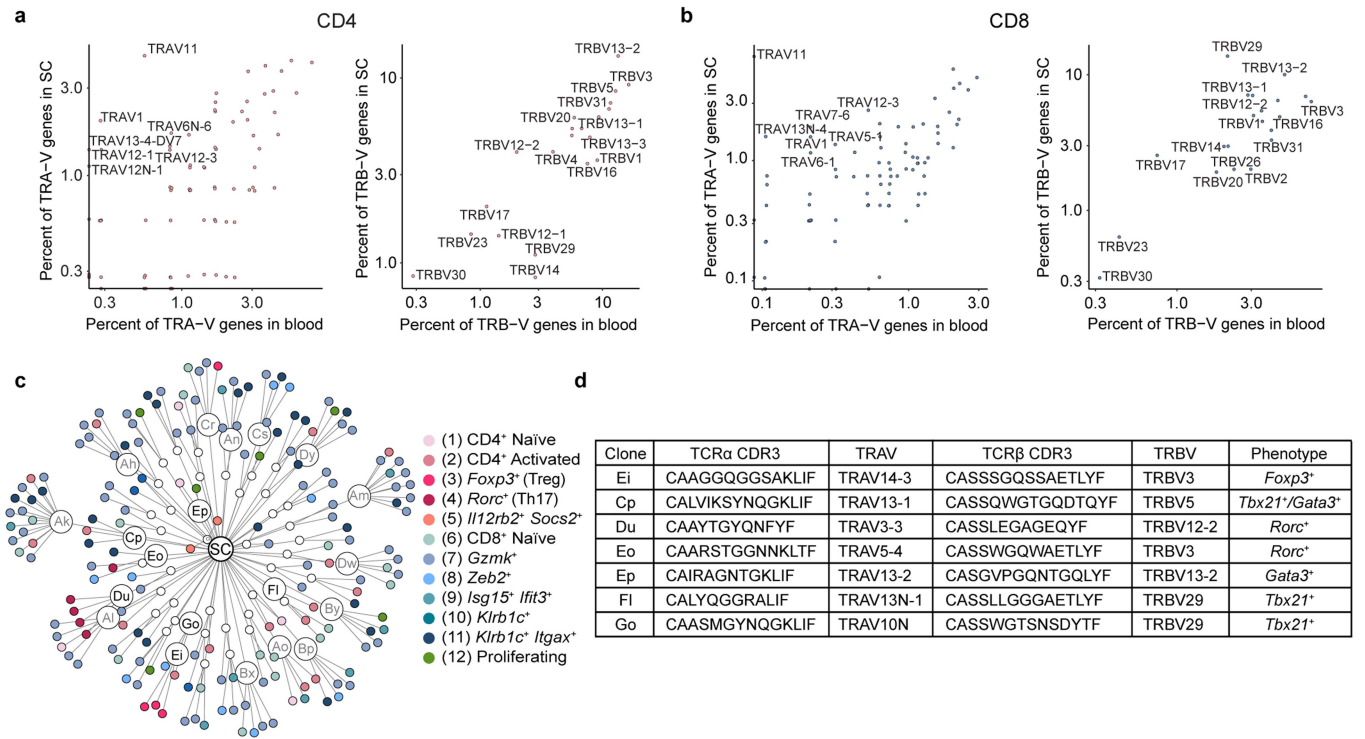
**Reprints and permissions information** is available at <http://www.nature.com/reprints>.



### Extended Data Fig. 1 | Phenotype of spinal cord infiltrating T cells.

**a, b**, Quantification of flow cytometry analysis for immune cells infiltrating the injured spinal cord (SC; with pia mater) or spinal cord meninges (SCM; dura mater) at specific time points after injury.  $n = 4$  mice per group. Data are presented as mean  $\pm$  s.e.m. **c**, Dot plot demonstrating scaled marker gene expression and percentage of cells expressing these genes in each cluster of T cells. **d**, Bar graph showing cluster proportions of tissue infiltrating T cells in

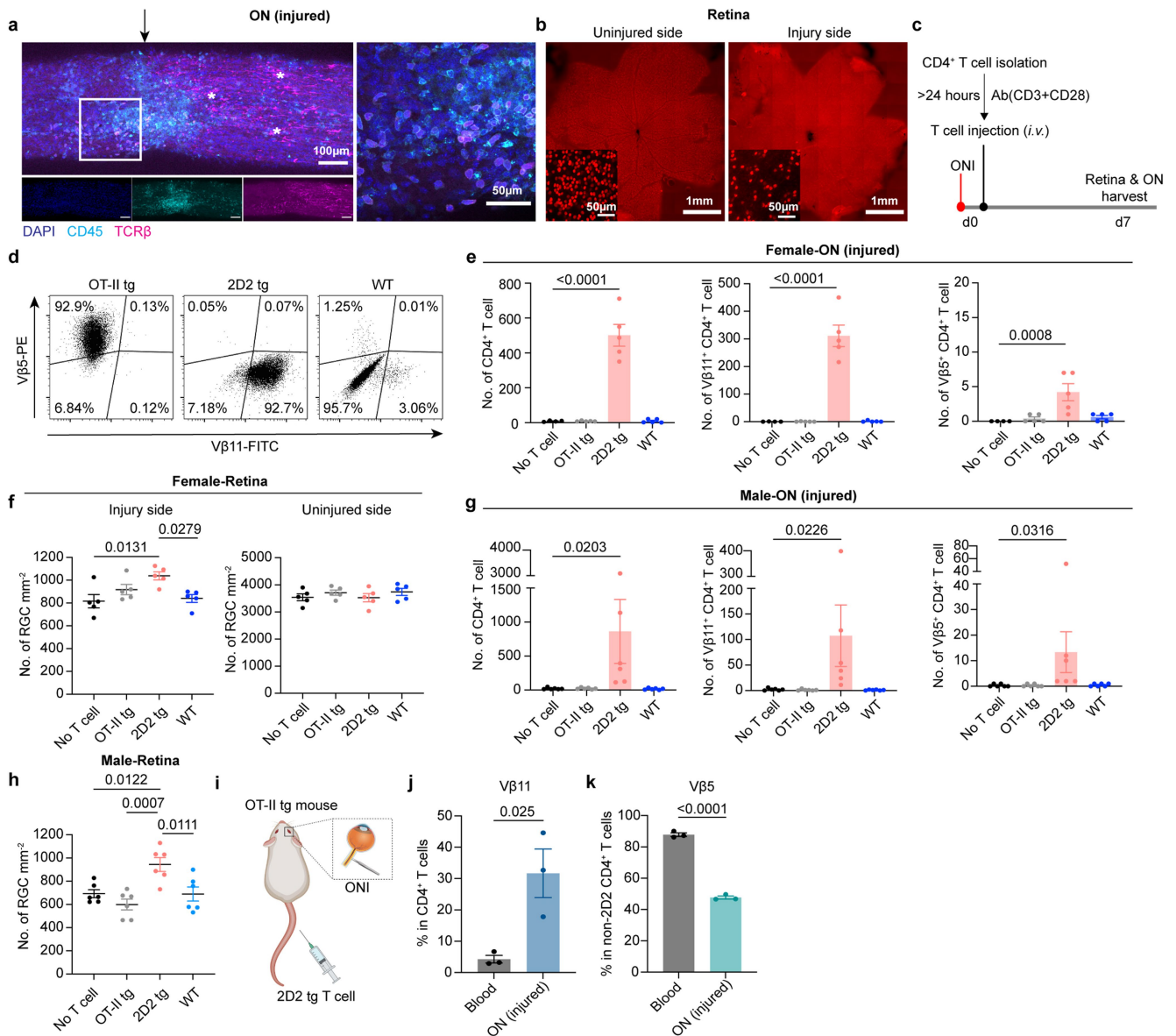
each group. **e**, Statistical analysis of T cells isolated from injured spinal cord ( $n = 30$  mice) or homeostatic blood ( $n = 5$  mice) of each T cell cluster. Data are presented as mean  $\pm$  s.e.m. f.c., fold change. **f**, UMAP visualization of scRNA-seq analysis of T cells based on CD4<sup>+</sup> or CD8<sup>+</sup> subtype. **g**, Violin plots showing the expression levels of *Cd4* and *Cd8b1* in CD4<sup>+</sup> and CD8<sup>+</sup> groups. **h**, UMAP visualization of the scaled average expression of specific genes of T cell subtypes.



**Extended Data Fig. 2 | Clonality of spinal cord infiltrating T cells. a, b,** Dot plot representation for the enrichment of TCR V $\alpha$  and V $\beta$  subtypes of CD4<sup>+</sup> T cells (a) and CD8<sup>+</sup> T cells (b), comparing TCRs from the injured spinal cord with TCRs from homeostatic blood. **c,** Q-plot visualization for each TCR clone (dots in white) and cells (dots with color) sharing same TCR sequences based on

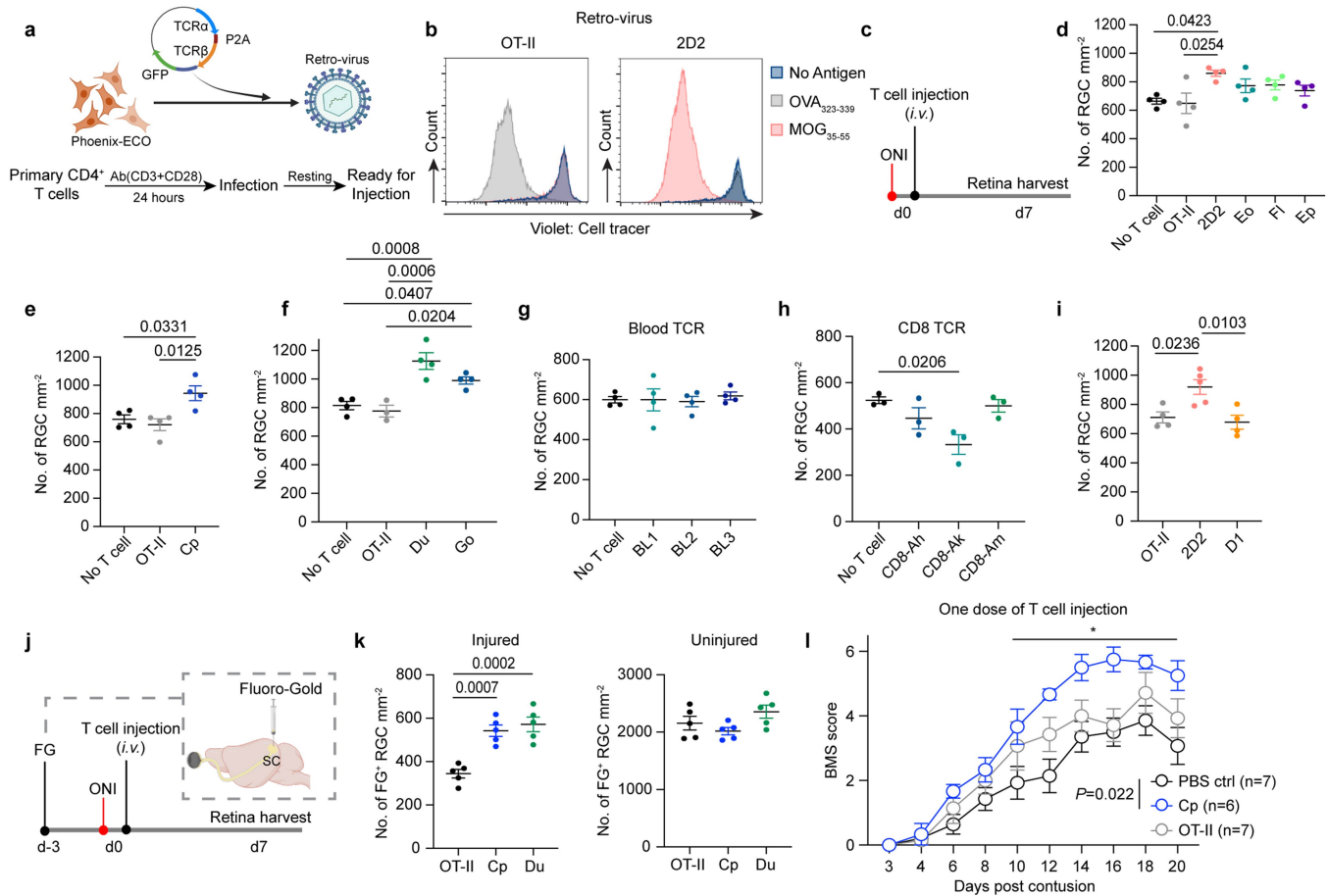
cluster transcriptional profile. All CD4<sup>+</sup> T cell clones (name in black) and CD8<sup>+</sup> T cell clones with higher clonality (more than three cells, name in grey) are highlighted. **d,** List of T cell phenotype, TCR subtype and sequences for the CDR3 regions of CD4<sup>+</sup> T cell clones from the injured spinal cord.





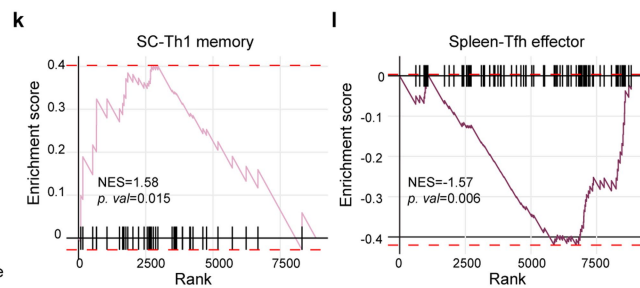
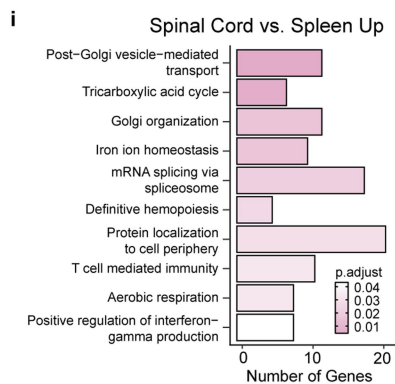
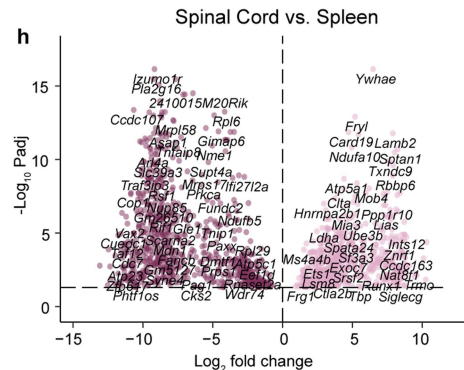
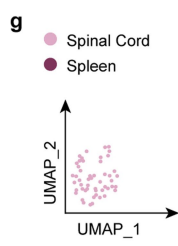
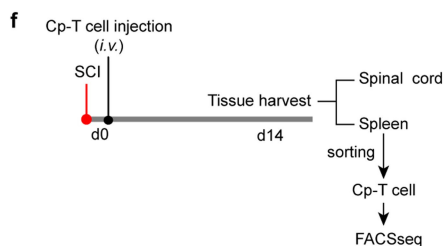
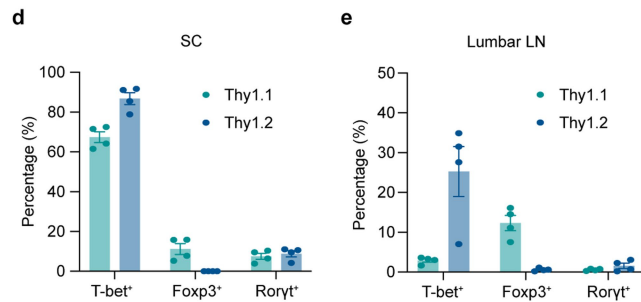
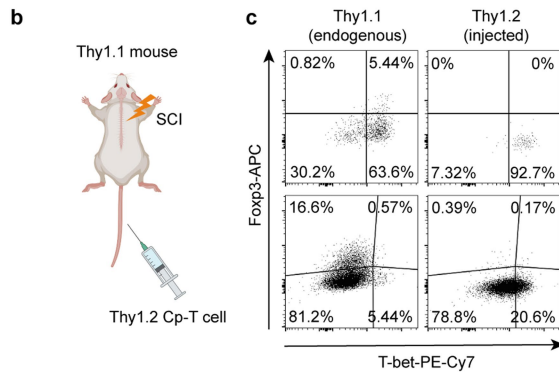
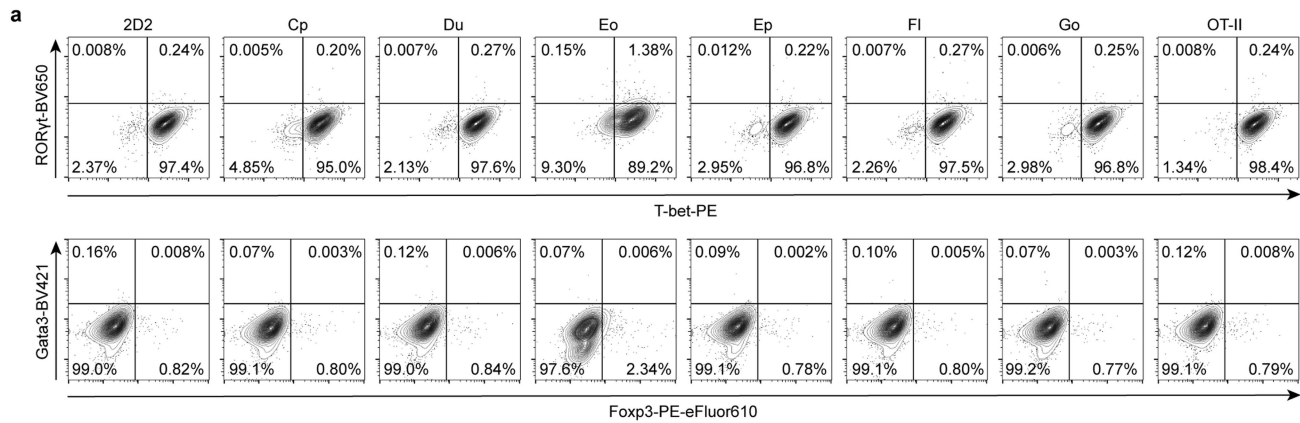
**Extended Data Fig. 3 | Neuroprotective function of self-reactive T cells in ONI.** **a**, Immunohistochemistry of the injured optic nerve 14 days after optic nerve injury. Arrow indicates the injury site. The area labeled with \* represents nonspecific staining of the TCR $\beta$  antibody. Inset represents enlarged area of interest. **b**, Whole-mount retina immunohistochemistry of Brn-3a<sup>+</sup> RGCs in the contralateral (uninjured) or ipsilateral (injury) side after optic nerve injury. Insets highlight enlarged regions with RGCs. **c**, Schematic representation for the optic nerve injury model to test the function of T cells isolated from OT-II, 2D2 TCR transgenic mice or WT mice. **d**, Flow cytometry analysis of CD4<sup>+</sup> T cells before injection. **e, g**, Quantification of flow cytometry analysis for T cell infiltration in the injured optic nerve in female and male mice.  $n = 5$  mice per group (lost one sample during processing in control group) for female and  $n = 6$

mice per group for male. Data are presented as mean  $\pm$  s.e.m. One-way ANOVA. **f, h**, Quantification of RGCs by Brn-3a staining to determine the neuroprotective function of T cells with different TCR expression in the optic nerve injury model. Each dot represents the averaged RGC number from each retina.  $n = 5$  mice per group for female and  $n = 6$  mice per group for male. Data are presented as mean  $\pm$  s.e.m. One-way ANOVA with Tukey's multiple comparison test. **i**, Schematic representation for inducing optic nerve injury on OT-II transgenic mice and injecting 2D2 tg T cell after injury. The diagram was created using BioRender (<https://biorender.com>). **j, k**, Quantification of flow cytometry result for 2D2 tg T cell (V $\beta$ 11<sup>+</sup>) infiltration and recruitment of OT-II tg T cells (V $\beta$ 5<sup>+</sup>) after optic nerve injury.  $n = 3$  mice per group. Data are presented as mean  $\pm$  s.e.m. Two-tailed unpaired Student's *t*-test.



**Extended Data Fig. 4 | Neuroprotective function of tissue infiltrating T cells.** **a**, Schematic representation of TCR reconstitution in primary CD4<sup>+</sup> T cells by retro-virus infection. The diagram was created using BioRender (<https://biorender.com>). **b**, T cell proliferation assays to test the function and specificity of reconstituted TCRs. CD4<sup>+</sup> T cells expressing TCR<sub>OT-II</sub> or TCR<sub>2D2</sub> (GFP<sup>+</sup>) were gated to assess the dilution of Cell Tracer Violet. **c**, Schematic representation of the optic nerve injury and T cell injection model to screen the neuroprotective function of T cells. **d**, **e**, **f**, Functional screening for spinal cord TCRs. Quantification of RGC number by Brn-3a staining after optic nerve injury and treatment with CD4<sup>+</sup> T cells carrying retrovirus delivered TCRs. Injury only, without T cell injection (No T cell) serves as a negative control. Each dot represents the averaged RGC number from each retina of a mouse. n = 3 or 4 mice per group. Data are presented as mean ± s.e.m. One-way ANOVA with Tukey's multiple comparison test. **g**, Quantification of RGC number by Brn-3a staining after optic nerve injury and treatment with CD4<sup>+</sup> T cells carrying reconstituted TCRs from blood of naïve mice. n = 4 mice per group. Data are presented as mean ± s.e.m. **h**, Quantification of RGC number by Brn-3a staining after optic nerve injury and treatment with CD8<sup>+</sup> T cells carrying reconstituted

TCRs from spinal cord CD8<sup>+</sup> T cell clones. n = 3 mice per group. Data are presented as mean ± s.e.m. One-way ANOVA with Tukey's multiple comparison test. **i**, Quantification of RGC number by Brn-3a staining after optic nerve injury and treatment with CD4<sup>+</sup> T cells carrying reconstituted TCR<sub>OT-II</sub>, TCR<sub>2D2</sub>, or a diaphragm TCR clone D1. n = 4 or 5 mice per group. Data are presented as mean ± s.e.m. One-way ANOVA with Tukey's multiple comparison test. **j**, Schematic representation of the ONI model using Fluoro-Gold (FG) injection to test the neuroprotective function of T cells. The diagram was created using BioRender (<https://biorender.com>). **k**, Quantification of FG<sup>+</sup> RGCs in the injury (ipsilateral) and uninjured (contralateral) side after ONI and treatment with CD4<sup>+</sup> T cells expressing different retrovirus delivered TCRs. n = 5 mice per group. Data are presented as mean ± s.e.m. One-way ANOVA with Tukey's multiple comparison test. **l**, The BMS score of SCI mice with injection of CD4<sup>+</sup> T cells carrying retrovirus delivered TCR<sub>Cp</sub> or TCR<sub>OT-II</sub>, with PBS treatment as control. Data are presented as mean ± s.e.m. \*P < 0.05, at individual time points between the PBS control group and the TCR<sub>Cp</sub> group (two-way ANOVA with Tukey's multiple comparison test).

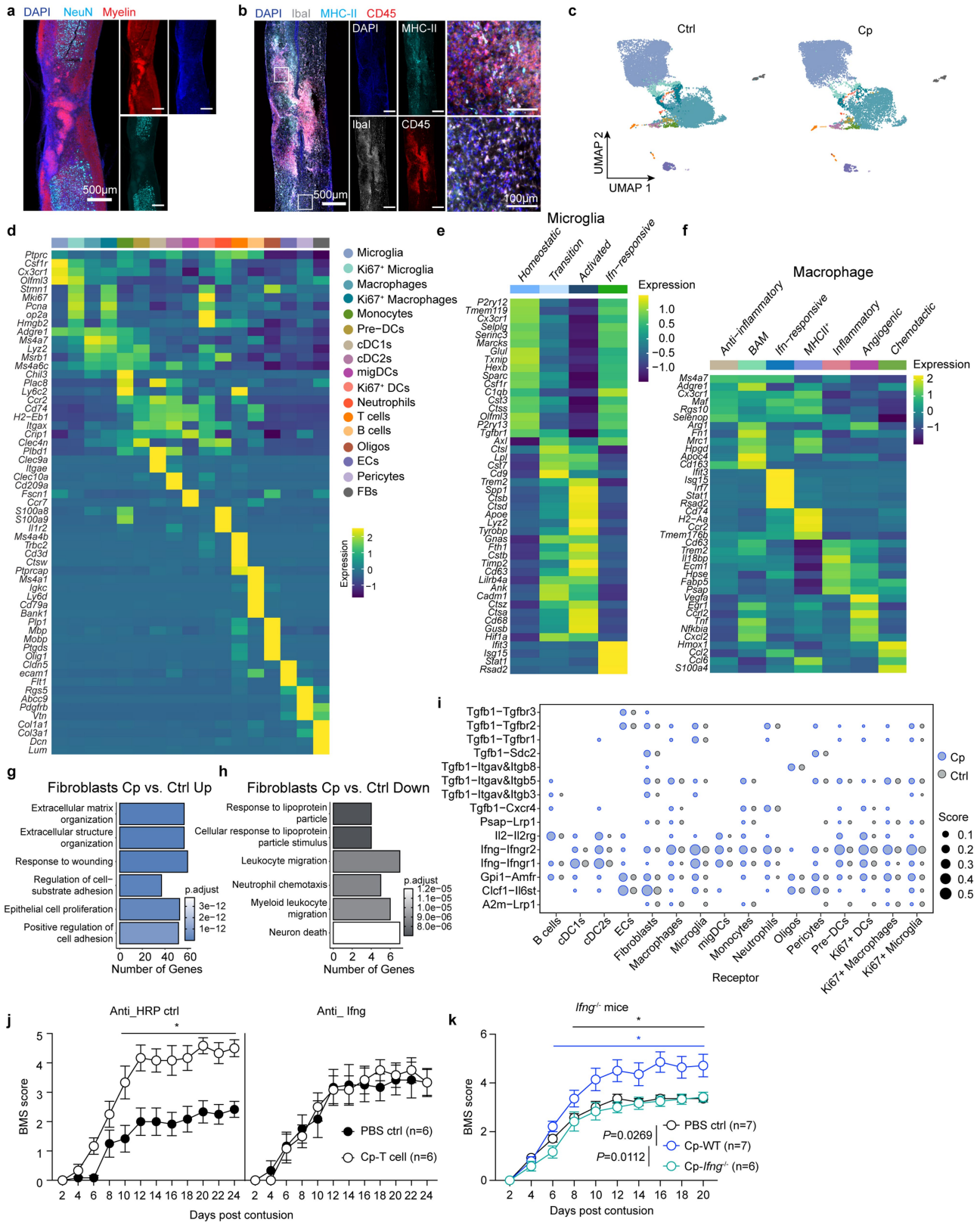


Extended Data Fig. 5 | See next page for caption.

# Article

**Extended Data Fig. 5 | Phenotype of neuroprotective T cells.** **a**, Flow cytometry analysis for in vitro cultured primary CD4<sup>+</sup> T cell with specific reconstituted TCRs before injection. Transcription factor of T cell subtypes Th1 (T-bet), Th2 (Gata3), Th17 (ROR $\gamma$ t), Treg (Foxp3) were tested. **b**, Schematic representation for inducing spinal cord injury on Thy1.1 mice and injecting Thy1.2 (WT) T cell after injury. The diagram was created using BioRender (<https://biorender.com>). **c**, Flow cytometry phenotyping of CD4<sup>+</sup> T cells in the spinal cord or lumbar lymph node (draining LN for spinal cord) 7 days after spinal cord injury. **d, e**, Quantification of flow cytometry phenotyping for CD4<sup>+</sup> T cells in the spinal cord or lumbar lymph node. Gate for single transcription factor was used for quantification.  $n = 4$  mice per group. Data are presented as mean  $\pm$  s.e.m. **f**, Schematic representation for FACS-seq analysis of TCR<sub>CP</sub> T cells in the injured spinal cord and the spleen.  $n = 6$  total mice were pooled for T cell isolation. **g**, UMAP visualization of FACS-seq of TCR<sub>CP</sub> T cells from the injured spinal cord vs. spleen. **h**, Volcano plots showing genes that were upregulated or

downregulated in TCR<sub>CP</sub> T cells when comparing the injured spinal cord to the spleen. P values were adjusted with the Benjamini-Hochberg method. F-test with adjusted degrees of freedom based on weights calculated per gene with a zero-inflation model. **i**, Top ten upregulated Gene Ontology terms comparing TCR<sub>CP</sub> T cells from the injured spinal cord with that in the spleen. P values were adjusted with the Benjamini-Hochberg method. Over-representation test. **j**, Gene Set Enrichment Analysis (GSEA) Hallmark analysis showing enriched gene sets associated with T cell phenotype in TCR<sub>CP</sub> T cells isolated from injured spinal cord and spleen. P values were determined by GSEA software. **k, l**, Enrichment plots for top one data set enriched in GSEA Hallmark analysis, representing differentially expressed genes associated with Th1 memory cells or Tfh effector cells. P values and normalized enrichment score (NES) were determined by GSEA software. Values with positive NES indicates enrichment in spinal cord T cells, negative NES value indicates enrichment in spleen.



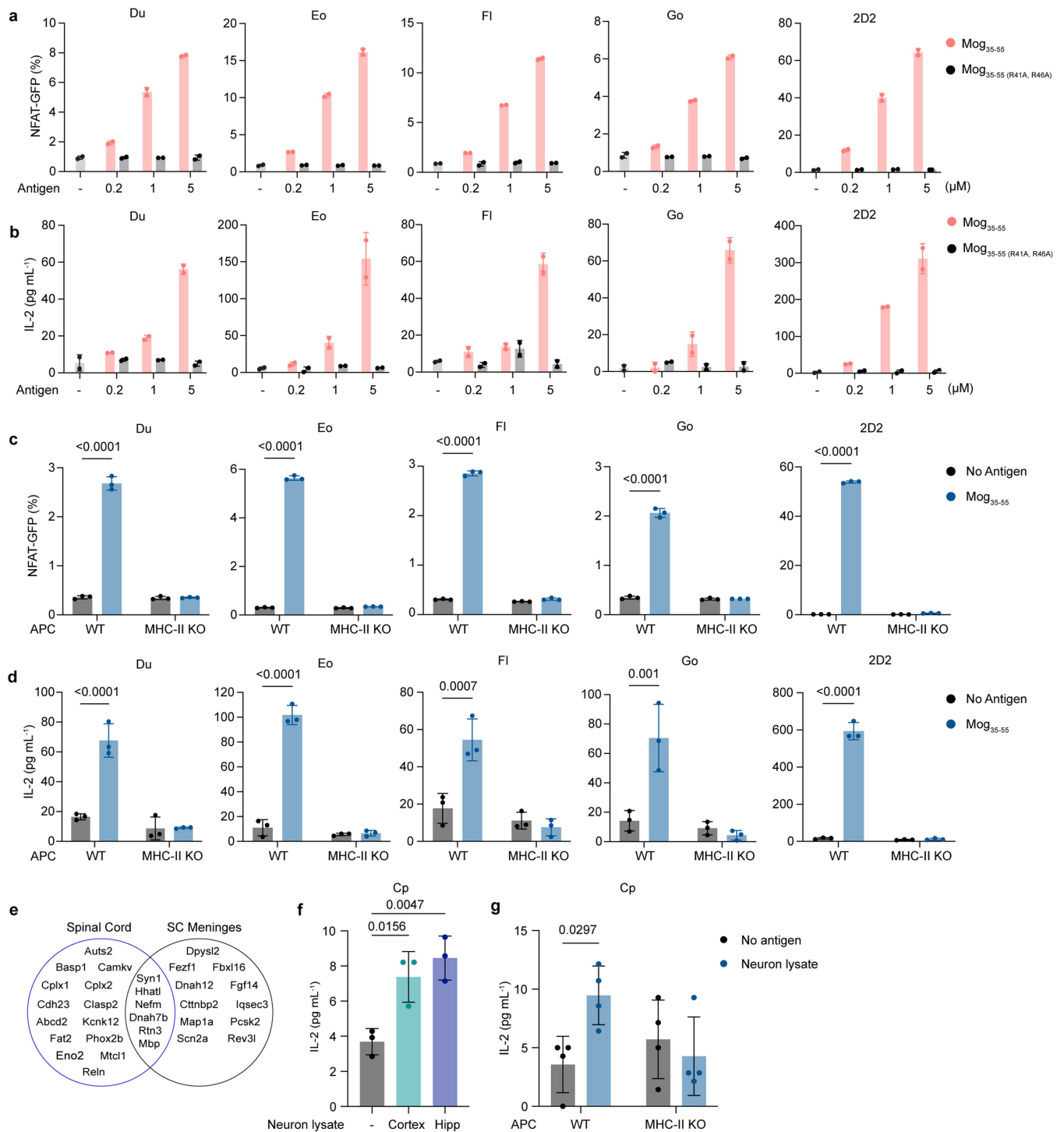
Extended Data Fig. 6 | See next page for caption.



# Article

**Extended Data Fig. 6 | Neuroprotective T cells tune local immune response through IFN $\gamma$ .** **a**, Immunohistochemistry of neurons and myelin sheath in the scar region of the spinal cord 7 days after injury. Experiment was repeated twice, and one representative result is shown. **b**, Immunohistochemistry of immune cells in the scar region of the spinal cord 7 days after injury. Insets represent an enlarged region of the injury site and a region close to injury site separately. Experiment was repeated twice, and one representative result is shown. **c**, UMAP visualization of scRNA-seq analysis of purified CD45<sup>+</sup> cell populations after SCI based on cell types. **d**, Heatmap demonstrating expression of marker genes in each cell cluster of CD45<sup>+</sup> population. **e**, **f**, Heatmap demonstrating the expression of marker genes in each sub-cluster of microglia and macrophage. **g**, **h**, Six upregulated or downregulated Gene Ontology terms with significance comparing the TCR<sub>Cp</sub> treatment group with control group in fibroblasts. P values were adjusted with the Benjamini-Hochberg method.

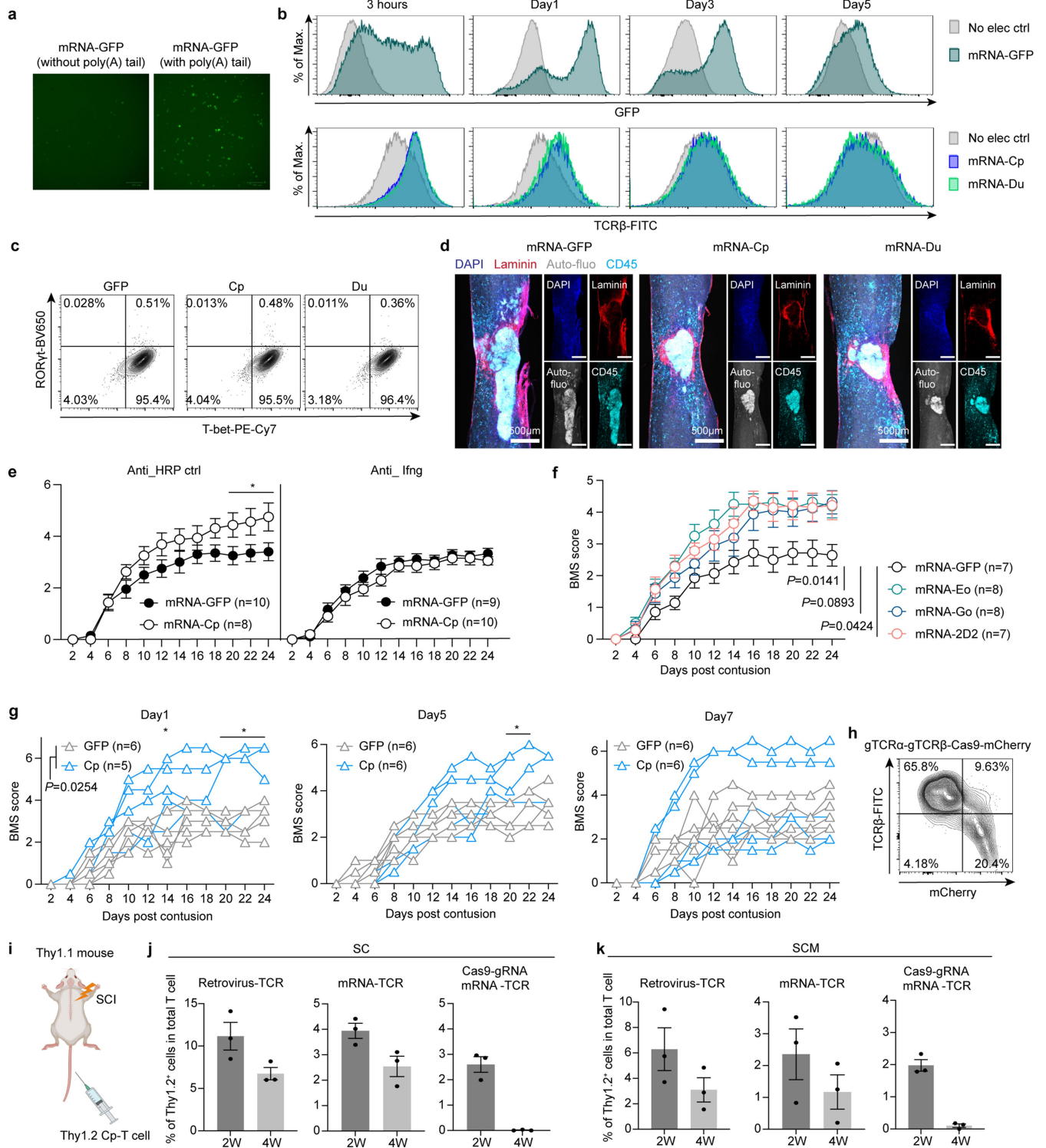
Over-representation test. **i**, Dot plot demonstrating scaled ligand-receptor pairs in each cell cluster comparing the TCR<sub>Cp</sub> group with control group. **j**, BMS score of mice after IFN $\gamma$  antibody neutralization, SCI, and injections with TCR<sub>Cp</sub> T cells, with antibody targeting HRP treatment as control. Antibody was injected every 5 days for 4 times (day -1, day 4, day 9, day 14). Data are presented as mean  $\pm$  s.e.m. \* $P < 0.05$ , at individual time points between TCR<sub>Cp</sub> group and control group (two-way ANOVA with Tukey's multiple comparison test). **k**, BMS score of *Irfng*<sup>-/-</sup> mice following SCI and subsequent injections with TCR<sub>Cp</sub> T cells derived from either WT or *Irfng*<sup>-/-</sup> backgrounds, with PBS treatment serving as the control. Data are presented as mean  $\pm$  s.e.m. \* $P < 0.05$ , at individual time points between groups (two-way ANOVA with Tukey's multiple comparison test). Significance in black represents difference between Cp-WT group with PBS control and significance in blue represents difference between Cp-WT group with Cp-*Irfng*<sup>-/-</sup> group.



### Extended Data Fig. 7 | Antigen specificity of injury associated T cells.

**a, b**, NFAT-GFP quantification by flow cytometry analysis and IL-2 ELISA quantification showing activation of reporter hybridomas with specific TCR expression after co-culturing with different concentration of Mog<sub>35-55</sub> or mutated Mog<sub>35-55</sub>(R41A, R46A) peptides. Experiments were repeated at least twice, and one representative result is shown. Data are represented as mean  $\pm$  s.d.,  $n = 2$  technical replicates. **c, d**, NFAT-GFP quantification by flow cytometry analysis and IL-2 ELISA quantification showing activation of reporter hybridomas with specific TCR expression after co-culturing with 5  $\mu$ M of Mog<sub>35-55</sub> and APCs isolated from WT or MHC-II knock out mice. Experiments were repeated twice, and one representative result is shown. Data are represented as mean  $\pm$  s.d.,  $n = 3$  technical replicates. Two-way ANOVA with Tukey's multiple comparison test. **e**, Lists showing the name of CNS-elevated

proteins targeted by MHC-II binding peptides in the injured spinal cord and spinal cord meninges (dura mater). **f**, IL-2 ELISA result showing activation of reporter hybridomas expressing TCR<sub>Cp</sub> after co-culturing with APCs and primary neuronal lysates (2 mg mL<sup>-1</sup> wet cell pellet) derived from specific brain region. Experiment was repeated three times, and one representative result is shown. Data are represented as mean  $\pm$  s.d.,  $n = 3$  technical replicates. One-way ANOVA with Dunnett's multiple comparison test. **g**, IL-2 ELISA result showing activation of reporter hybridoma expressing TCR<sub>Cp</sub> after co-culturing with primary neuronal lysates and APCs isolated from WT or MHC-II knock out mice. Experiment was repeated three times, and one representative result is shown. Data are represented as mean  $\pm$  s.d.,  $n = 4$  technical replicates. Two-way ANOVA with Sidak's multiple comparison test.

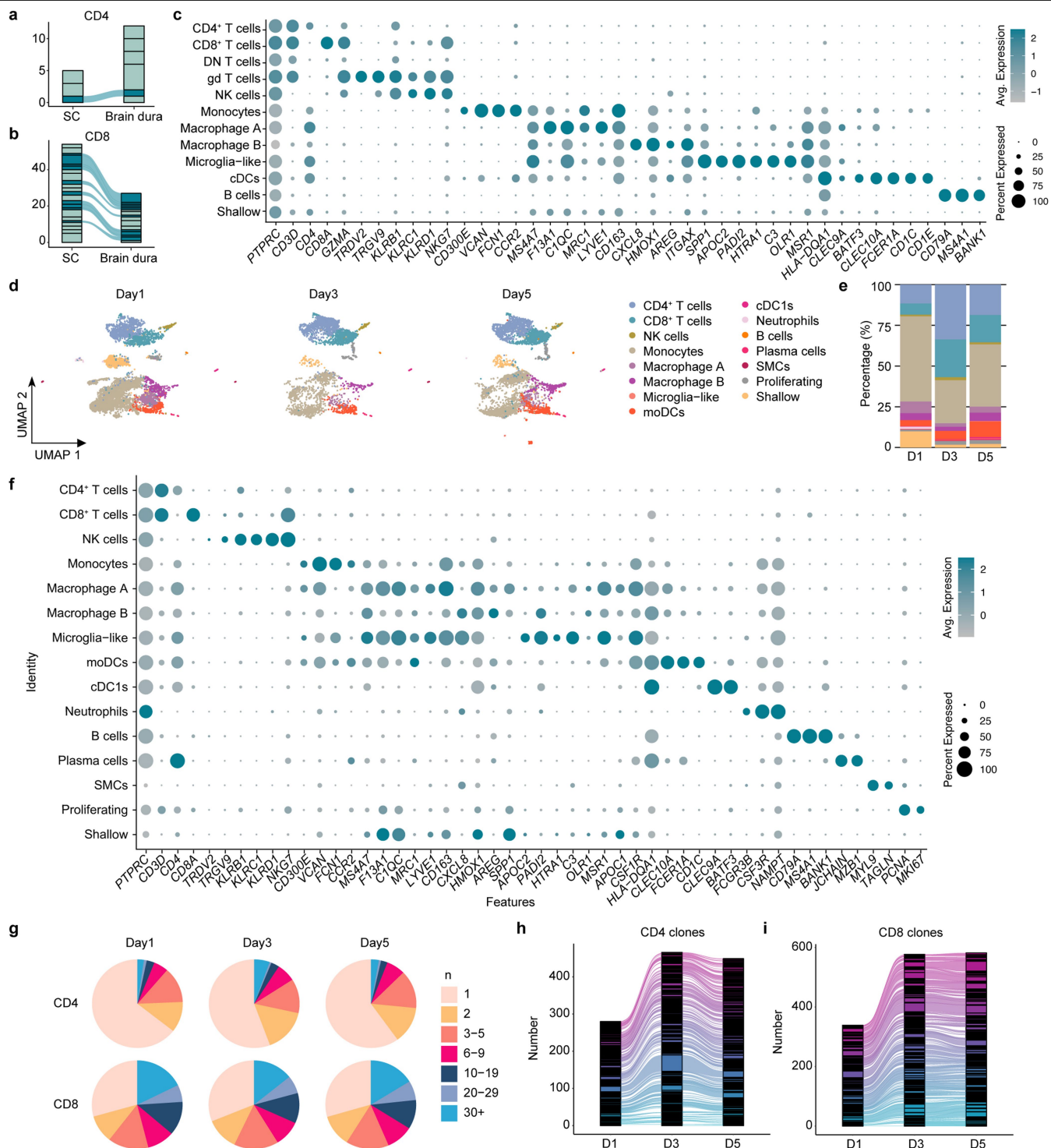


**Extended Data Fig. 8** | See next page for caption.

**Extended Data Fig. 8 | mRNA-TCR based T cell therapy for CNS injury.**

**a**, Image showing GFP expression in primary CD4<sup>+</sup> T cells 4 h after GFP mRNA electroporation. Electroporation of mRNA without poly (A) tail as negative control. Experiment with same control group was only done once. **b**, Time course performed by flow cytometry analysis to determine the life span of mRNA-based GFP and TCR expression. **c**, Flow cytometry analysis of phenotyping in vitro cultured primary CD4<sup>+</sup> T cell with mRNA delivered TCRs. **d**, Immunohistochemistry showing infiltration of CD45<sup>+</sup> immune cells and extracellular matrix components in the scar region of the spinal cord 4 weeks after injury with treatment of CD4<sup>+</sup> T cells expressing mRNA-based TCR<sub>Cp</sub>, TCR<sub>Du</sub> or GFP. Experiment was repeated at least twice. **e**, BMS score of mice after IFN $\gamma$  antibody neutralization, SCI, and injections with mRNA-based TCR<sub>Cp</sub> T cells, with antibody targeting HRP treatment as control. Antibody was injected every 5 days for 3 times (day -1, day 4, day 9). Data are presented as mean  $\pm$  s.e.m. \* $P$  < 0.05, at individual time points between mRNA-Cp group and control group (two-way ANOVA with Tukey's multiple comparison test). **f**, BMS score of SCI mice after injury with treatment of CD4<sup>+</sup> T cells carrying

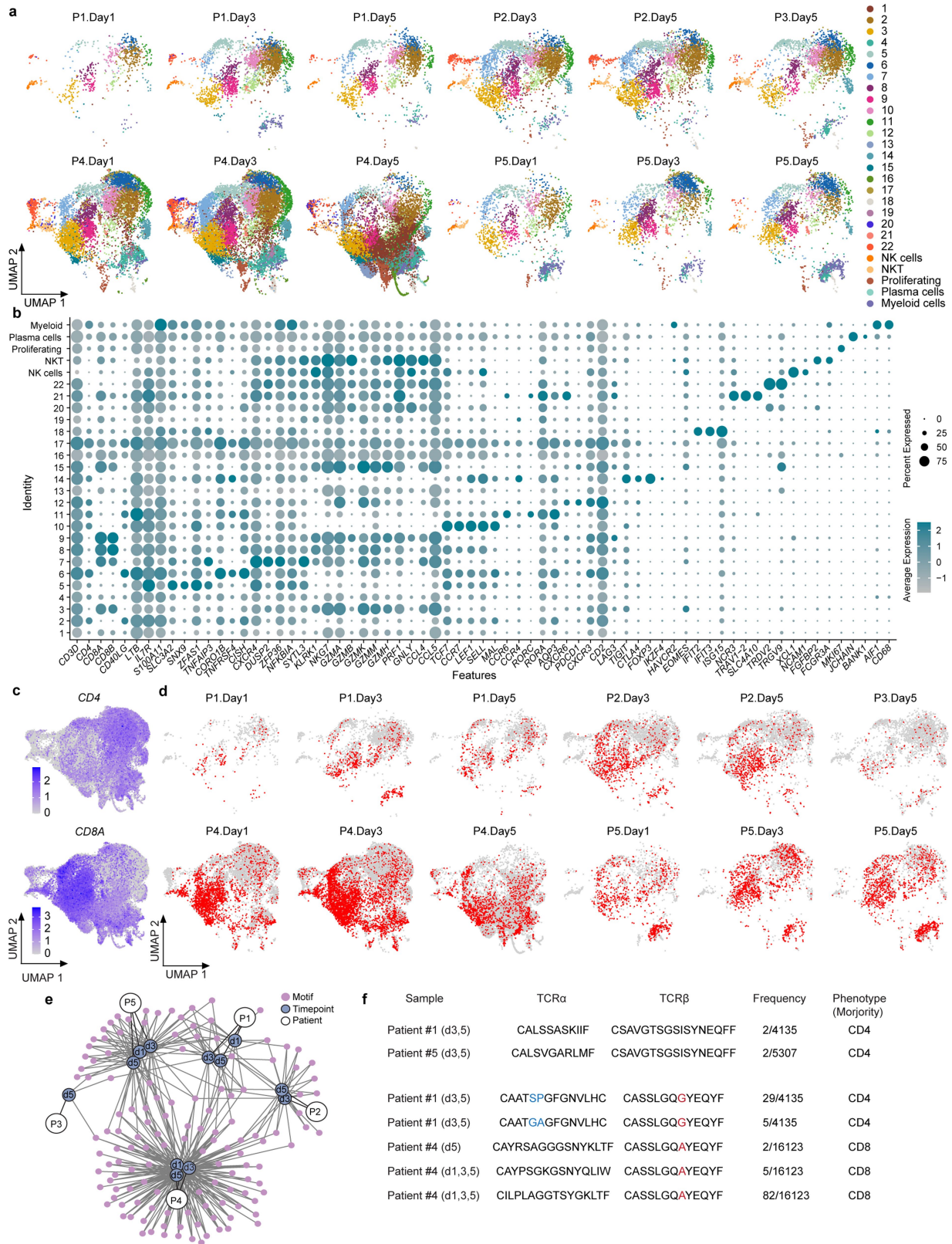
mRNA-based TCRs. Data are presented as mean  $\pm$  s.e.m. Two-way ANOVA with Tukey's multiple comparison test. **g**, BMS score of SCI mice after injury and treatment at different time point with CD4<sup>+</sup> T cells carrying mRNA-based TCR<sub>Cp</sub>. One dose of T cells was injected for each experiment. Data are presented as mean  $\pm$  s.e.m. \* $P$  < 0.05, at individual time points between mRNA-GFP control group and TCR<sub>Cp</sub> T cell treatment group (two-way ANOVA with Sidak's multiple comparison test). **h**, Flow cytometry analysis for endogenous TCR removal 2 days after electroporating a plasmid carrying Cas9, mCherry and guide-RNA targeting endogenous TCR $\alpha/\beta$ . **i**, Schematic representation for inducing spinal cord injury on Thy1.1 mice and injecting Thy1.2 (WT) T cell after injury. The diagram was created using BioRender (<https://biorender.com>). **j**, **k**, Quantification of flow cytometry analysis for infiltration of T cells expressing TCR<sub>Cp</sub> 2 weeks or 4 weeks after injury in the injured spinal cord (SC) or spinal cord meninges (SCM). The expression of TCR<sub>Cp</sub> is induced by retrovirus infection or mRNA electroporation in WT primary T cells, or in T cells with endogenous TCR removal.  $n = 3$  mice per group. Data are presented as mean  $\pm$  s.e.m.



**Extended Data Fig. 9 | Phenotype and clonality of CSF-derived T cells from individual patients with spinal cord injury.** **a, b,** Alluvial plot showing shared CD4<sup>+</sup> or CD8<sup>+</sup> TCRs between injured spinal cord and brain meninges (dura mater) of SCI mice. **c,** Dot plot demonstrating scaled marker gene expression and percentage of cells expressing these genes in each cell cluster. **d,** UMAP visualizations of scRNA-seq analysis of total cells in human CSF sampled at different time points post-cervical SCI, color-coded by cell type. **e,** Bar graph

showing proportions of each cell type at different time points post-cervical SCI. **f,** Dot plot demonstrating scaled marker gene expression and percentage of cells expressing these genes in each cell cluster. **g,** Pie graphs showing the proportions of CD4<sup>+</sup> and CD8<sup>+</sup> T cell clones in human CSF samples at different time points post-cervical SCI. **h, i,** Alluvial plots showing shared CD4<sup>+</sup> or CD8<sup>+</sup> TCR clones in human CSF sample at different time points post-cervical SCI.





**Extended Data Fig. 10 | Phenotype and clonality of CSF-derived T cells combined from spinal cord injury patients.** **a**, UMAP visualizations of scRNA-seq analysis of total T cells in human CSF plotted by individual sample. **b**, Dot plot demonstrating scaled marker gene expression and percentage of cells expressing these genes in each cell cluster. **c**, UMAP visualization of the scaled average expression of *CD4* and *CD8A* in T cells. **d**, UMAP visualization

of T cell clonality plotted by individual sample, red dots represent cells with clonality, grey dots represent single clones. **e**, Q-plot visualization of information for TCR clones sharing motif similarity of TCRβ among or between patients and time points. **f**, List detailing TCR information for T cell clone sharing the same TCRβ CDR3 sequence between patients (above) and the top one T cell clone sharing motif similarity between patients (below).

## Reporting Summary

Nature Portfolio wishes to improve the reproducibility of the work that we publish. This form provides structure for consistency and transparency in reporting. For further information on Nature Portfolio policies, see our [Editorial Policies](#) and the [Editorial Policy Checklist](#).

### Statistics

For all statistical analyses, confirm that the following items are present in the figure legend, table legend, main text, or Methods section.

n/a Confirmed

- The exact sample size ( $n$ ) for each experimental group/condition, given as a discrete number and unit of measurement
- A statement on whether measurements were taken from distinct samples or whether the same sample was measured repeatedly
- The statistical test(s) used AND whether they are one- or two-sided  
*Only common tests should be described solely by name; describe more complex techniques in the Methods section.*
- A description of all covariates tested
- A description of any assumptions or corrections, such as tests of normality and adjustment for multiple comparisons
- A full description of the statistical parameters including central tendency (e.g. means) or other basic estimates (e.g. regression coefficient) AND variation (e.g. standard deviation) or associated estimates of uncertainty (e.g. confidence intervals)
- For null hypothesis testing, the test statistic (e.g.  $F$ ,  $t$ ,  $r$ ) with confidence intervals, effect sizes, degrees of freedom and  $P$  value noted  
*Give  $P$  values as exact values whenever suitable.*
- For Bayesian analysis, information on the choice of priors and Markov chain Monte Carlo settings
- For hierarchical and complex designs, identification of the appropriate level for tests and full reporting of outcomes
- Estimates of effect sizes (e.g. Cohen's  $d$ , Pearson's  $r$ ), indicating how they were calculated

*Our web collection on [statistics for biologists](#) contains articles on many of the points above.*

### Software and code

Policy information about [availability of computer code](#)

Data collection

The following softwares were used to collect the data in this study:

- Olympus V200 ASW
- CYTEK SpectroFlo
- Leica Application Suite v4.3.0.24308
- BioTek Gen5 3.11
- Illumina NextSeq Control Software
- Thermo Scientific Orbitrap Fusion Lumos Control Software
- Cellranger\_1.1.0

Data analysis

The following softwares were used to analyze the data in this study:

- Fiji image processing software v2.1.0/1.53c
- Prism v9.4.0
- SnapGene v4.3.6
- FlowJo v10.7.1
- R v3.5.0
- 10X genomics Cellranger software pipeline
- Seurat v3
- STAR v2.5.1a
- PEAKS Studio 10.6
- Custom code used for single-cell-seq analysis is available upon reasonable request.

- DropletUtils\_1.10.3

- Custom code used for single-cell RNA-seq analysis is available from the corresponding authors upon request.

For manuscripts utilizing custom algorithms or software that are central to the research but not yet described in published literature, software must be made available to editors and reviewers. We strongly encourage code deposition in a community repository (e.g. GitHub). See the Nature Portfolio [guidelines for submitting code & software](#) for further information.

## Data

Policy information about [availability of data](#)

All manuscripts must include a [data availability statement](#). This statement should provide the following information, where applicable:

- Accession codes, unique identifiers, or web links for publicly available datasets
- A description of any restrictions on data availability
- For clinical datasets or third party data, please ensure that the statement adheres to our [policy](#)

Adventitious Proteins database ([www.thegpm.org/crap/](http://www.thegpm.org/crap/))

Human Protein Atlas Database (<https://www.proteinatlas.org>)

Raw data of all single-cell sequencing are available on the Gene Expression Omnibus (GEO) under accession numbers GSE216391 and GSE189812.

Raw data of Mass Spec peptidome has been uploaded on MassIVE under accession numbers MSV000091130.

## Human research participants

Policy information about [studies involving human research participants and Sex and Gender in Research](#).

Reporting on sex and gender	Data from both male and female are involved. No preference of gender for the study.
Population characteristics	Cerebrospinal fluid (CSF) samples without obvious blood contamination are involved in the study. Five patients with complete/incomplete spinal cord injury were involved in this study. Patients involved in this study were with either thoracic or cervical spinal cord injury. Both male and female were involved in this study. Patients involved in this study were at their age of 20s to 70s.
Recruitment	Patients in Barnes-Jewish Hospital with complete/ incomplete spinal cord injury were involved in this study. These samples were obtained with informed consent for research use and were approved by the review board of Washington University in St. Louis.
Ethics oversight	The CSF samples used in the scRNA-seq experiments were obtained with informed consent for research use and were approved by the review board of Washington University in St. Louis under IRB# 202012050.

Note that full information on the approval of the study protocol must also be provided in the manuscript.

## Field-specific reporting

Please select the one below that is the best fit for your research. If you are not sure, read the appropriate sections before making your selection.

Life sciences       Behavioural & social sciences       Ecological, evolutionary & environmental sciences

For a reference copy of the document with all sections, see [nature.com/documents/nr-reporting-summary-flat.pdf](https://nature.com/documents/nr-reporting-summary-flat.pdf)

## Life sciences study design

All studies must disclose on these points even when the disclosure is negative.

Sample size	Sample sizes were chosen on the basis of standard power calculations (with $\alpha = 0.05$ and power of 0.8) performed for similar experiments that were previously published (Drieu et al., Nature 2022). In general, statistical methods were not used to re-calculate or predetermine sample sizes.
Data exclusions	For BMS scoring (locomotion test) of spinal cord injury mice, if obvious infection of mice was observed, data from that individual mice will be removed. If the BMS score of SCI mice reaches 2 within the first two days after surgery, it indicates surgical failure. Data from such mice will be excluded from the analysis.
Replication	Number of reliable reproductions of each experimental finding is stated in each Figure legend. For single cell sequencing, mice (number mentioned individually in manuscript) were pooled in each group and sequence together. Other experiments were replicated at least once.
Randomization	Statistical analysis and reproducibility subsection: Mice were allocated randomly to cages with no more than 5 mice per cage after been shipped to the vivarium. Animals from different cages, but within the same experimental group, were selected to assure randomization. Mice from the same cage were received different treatments (for example, if there are four experimental groups in one experiment, will keep 4 mice per cage with each of them in different groups). Treatment was given in a blind manner and could be identified by a corresponding ear tag.

For in vitro studies, cells from the same animal were harvested and subjects were randomly assigned into each experimental group. Treatments and controls were plated adjacent to one another.

### Blinding

For single cell sequencing, at least one investigator responsible for sample collection was not blinded to ensure there was no cross-contamination between groups. Analyzer analyzed the data in blind.  
For optic nerve injury, treatments were given in a blind manner and analyzer analyzed data in blind. For spinal cord injury and BMS scoring, treatments were given in a blind manner and BMS scoring was performed every other day by two independent investigators, both of whom were blinded.  
No blinding was performed in the in vitro cell culture study to ensure there was no cross-contamination between groups.

## Reporting for specific materials, systems and methods

We require information from authors about some types of materials, experimental systems and methods used in many studies. Here, indicate whether each material, system or method listed is relevant to your study. If you are not sure if a list item applies to your research, read the appropriate section before selecting a response.

### Materials & experimental systems

### Methods

- | n/a                                 | Involved in the study   |
|-------------------------------------|---|
| <input type="checkbox"/>            | <input checked="" type="checkbox"/> Antibodies                  |
| <input type="checkbox"/>            | <input checked="" type="checkbox"/> Eukaryotic cell lines       |
| <input checked="" type="checkbox"/> | <input type="checkbox"/> Palaeontology and archaeology          |
| <input type="checkbox"/>            | <input checked="" type="checkbox"/> Animals and other organisms |
| <input checked="" type="checkbox"/> | <input type="checkbox"/> Clinical data                          |
| <input checked="" type="checkbox"/> | <input type="checkbox"/> Dual use research of concern           |

- | n/a                                 | Involved in the study                              |
|-------------------------------------|--|
| <input checked="" type="checkbox"/> | <input type="checkbox"/> ChIP-seq                  |
| <input type="checkbox"/>            | <input checked="" type="checkbox"/> Flow cytometry |
| <input checked="" type="checkbox"/> | <input type="checkbox"/> MRI-based neuroimaging    |

## Antibodies

### Antibodies used

Anti-CD45 (103124, BioLegend), anti-MHC-II (107650, BioLegend), anti-CD3 (50-0032-82, eBioscience), anti-Ibal (ab5076, Abcam), anti-Laminin (ab11575, Abcam), anti-GFAP (Z0334, Agilent Technologies), anti-Brn3a (411003, Synaptic system), anti-NeuN (ab190195, Abcam) and FluoroMeylin Red (F34652, Fisher Scientific) were used for immunostaining.  
Anti-CD3e (553057, BD Biosciences) and anti-CD28 (553294, BD Biosciences) were used for in vitro T cell activation.  
Flow cytometry antibodies of CD45-FITC (11-0451-85), CD90.2-PE-Cy7 (25-0902-81), CD4-APC-eFluor780 (47-0041-82), CD8-APC-eFluor780 (47-0081-82), CD3-eFluor660 (50-0032-82), CD69-APC-eFluor780 (47-0691-82), CD8a-Alexa Fluor 532 (58-0081-80), CD45-BV750 (746947), TCR $\beta$ -BUV805 (748405), B220-APC (50-0452-82), TCR $\gamma$ -FITC (11-5711-82), CD8a-Alexa Fluor 700 (557959), T-bet-PE (12-5825-82), T-bet-PE-Cy7 (25-5825-82), FoxP3-PE-eFluor610 (61-5773-82) FoxP3-APC (17-5773-80) and ROR $\gamma$ t-BV650 (BDB564722) were purchased from eBioscience/ Thermo Fisher. Flow cytometry antibodies of CD11b-PE-Cy7 (552850), CD45-APC (559864), CD4-PE (553049), B220-PE (553090), V $\beta$ 5-PE (553190), CD4-PE-Cy7 (552775), CD11c-PE-Cy7 (558079) and CD4-BUV395 (563790) were purchased from BD Biosciences. Flow cytometry antibodies of TCR $\beta$ -PerCP/Cy5.5 (109228), CD45-BV510 (103137), CD45-PE (103106), CD11b-PerCP/Cy5.5 (101228), CD3-Alexa Fluor 594 (100240), TCR $\beta$ -BV421 (109230), TCR $\beta$ -FITC (109206), MHCII-BV650 (107641), Thy1.2-BV510 (105335), Thy1.1-PE (202524), V $\beta$ 11-FITC (125905), CD62L-BV785 (104440), TCR $\beta$ -BV510 (109233), CD69-PE (104508), CD44-PerCP/Cy5.5 (103032), Gata3-BV421 (653813), Gata3-APC (653806), IFN $\gamma$ -BV711 (505836), Zombie Aqua (423102) and Zombie NIR Fixable Viability Kit (423105) were purchased from BioLegend. Antibodies for testing human CSF cells, HLA-DR (307638), TCR $\beta$ -BV785 (306741), CD8-APC-Cy7 (344713), CD4-APC-Fire 810 (344661), CD4-BV711 (300558), CD45-Alexa Fluor647 (304020) were purchased from BioLegend and CD11b-BUV563 (741242), CD235A-BUV395 (563810), CD5-BV421 (562646) were purchased from BD Biosciences.

### Validation

Each antibody was validated for the species (mouse, human) and application (immunohistochemistry, Flow cytometry and fluorescence activated cell sorting, cell culture) by the correspondent manufacturer. All of antibody were tested using samples from control tissue (for example, spleen and blood).

## Eukaryotic cell lines

Policy information about [cell lines and Sex and Gender in Research](#)

### Cell line source(s)

Phoenix-ECO retroviral packaging cells (CRL-3214) were obtained from the American Type Culture Collection (ATCC). The S8  $\alpha$ - $\beta$ - hybridoma was generated by Dr. Kenneth Murphy and kindly provided by Dr. Dan Littman (New York University, United State).  
Primary murine T cells: Spleen and lymph nodes from adult C57BL/6J mice were harvested, and primary CD4+ T cells were isolated using the EasySep mouse CD4+ T cell isolation kit (19852, STEMCELL Technologies). Both male and female were used depend on experimental design.  
Primary murine neuron: The brain of E15-E19 embryo of C57BL/6J mice were used for primary neuron culturing. Both male and female were used.

### Authentication

Primary murine CD4 T cells were identified by flow cytometry.  
Identity of other cell lines by checking cellular morphological features but have not been authenticated by the short tandem repeat (STR) profiling.

Mycoplasma contamination

Morphological features of cells were frequently checked but mycoplasma contamination was not checked by PCR.

Commonly misidentified lines  
(See [ICLAC](#) register)

No commonly misidentified cell lines are used in this study.

## Animals and other research organisms

Policy information about [studies involving animals](#); [ARRIVE guidelines](#) recommended for reporting animal research, and [Sex and Gender in Research](#)

Laboratory animals

Wild type C57BL/6J mice (JAX: 000664, 7-10 weeks old) were purchased from the Jackson Laboratory and were kept in-house for at least 1 week before the start of an experiment. OT-II TCR transgenic mice (JAX: 004194), and 2D2 TCR transgenic mice (JAX: 006912), Ifng<sup>-/-</sup> mice (JAX: 002287), Thy1.1 mice (JAX: 000406), Rosa26-Cas9 mice (JAX: 026179) were purchased from the Jackson Laboratory and bred in-house. Both male and female were used in this study. All mice were housed and bred in a temperature-controlled (22 °C) and humidity-controlled (33–39%) environment under a 12 h–12 h light–dark cycle and were provided with food and water ad libitum. No more than five mice were housed together per cage. Mice at their age between 2 months–4 months old were used.

Wild animals

No wild animal was involved in this study.

Reporting on sex

Only use female mice for spinal cord injury since spinal cord injury potentially induces urinary tract infection of male mice. Both male and female are involved in other experiments.

Field-collected samples

The study did not involve samples collected from the field.

Ethics oversight

All experiments were approved by the Institutional Animal Care and Use Committee of the Washington University in St. Louis.

Note that full information on the approval of the study protocol must also be provided in the manuscript.

## Flow Cytometry

### Plots

Confirm that:

- The axis labels state the marker and fluorochrome used (e.g. CD4-FITC).
- The axis scales are clearly visible. Include numbers along axes only for bottom left plot of group (a 'group' is an analysis of identical markers).
- All plots are contour plots with outliers or pseudocolor plots.
- A numerical value for number of cells or percentage (with statistics) is provided.

### Methodology

Sample preparation

Mice were injected with a lethal dose of Euthasol (10% vol/vol) and transcardially perfused with PBS containing 0.025% heparin. Lymph nodes and spleen were directly collected using forceps. For spinal cord isolation, the spine was cut on both sides and the spinal cord was flushed out using a PBS filled syringe with a 18-gauge needle. The muscles were then removed and spinal cord dura was peeled from the vertebral. Optic nerves from the eye to the optic chiasm were collected for the following research. Lymph nodes and spinal cord dura were directly digested at 37 °C for 30 minutes in prewarmed digestion buffer (RPMI-1640 medium supplemented with 2% FBS, 1 mg mL<sup>-1</sup> Collagenase VIII, and 0.5 mg mL<sup>-1</sup> of DNase I). Spinal cord was minced using a surgical blade and digested in digestion buffer at 37 °C for 30 minutes, triturated with a 1 mL pipette, and digested for another 15 minutes. For the spleen, digestion buffer was injected into the tissue parenchyma and incubated at 37 °C for 5 minutes. Then spleen was then minced with a surgical blade and digested in digestion buffer at 37 °C for 20 minutes. After digestion, enzymes were neutralized with RPMI with 10% FBS and tissue samples were mechanically homogenized and filtered through 70 µm cell strainer. Cells were then centrifuged at 450 g for 4 minutes and the supernatant was removed. For lymph nodes, the cell pellet was directly resuspended with RPMI containing 10% FBS and kept on ice until use. For the spleen, red blood cells were lysed with ammonium-chloridepotassium (ACK) lysis buffer for 1 minute at room temperature and neutralized with the same volume of RPMI containing 10% of FBS. Cells were then centrifuged and cell pellets were resuspended with RPMI containing 10% FBS and kept on ice until use. For spinal cord and spinal cord dura, myelin was removed by resuspending cells with 30% percoll or 10-15% BSA in PBS and centrifuged at 800 g for 10 minutes with a slow brake. After centrifugation, the upper myelin-containing layer and supernatant were removed, and the cell pellet was resuspended with RPMI containing 10 % FBS.

Single-cell suspensions were washed with PBS. The Zombie Aqua or Zombie NIR fixable Viability kit or DAPI was used to determine cell viability. Cell viability dyes were diluted in PBS and incubated with cells for 10 minutes at room temperature. After viability staining, Fc receptors were blocked for 5 min with the anti-CD16/CD32 antibody cocktail and cells were incubated with primary antibody cocktails for 10 minutes at room temperature for surface staining. Antibodies were all diluted in FACS buffer (2% BSA, 1 mM EDTA, 20 mM HEPES in PBS). After staining, samples were filtered with 70 µm cell strainer and ready for sample loading.

Instrument

Aurora spectral flow cytometer (Cytek)  
BD Biosciences FACSaria II



Software	CYTEK SpectroFlo for data collection. FlowJo v10.7.1 for data analyze.
Cell population abundance	Control cells or control tissue were always used for gating. For cell line study, post-sorted cells were cultured and purity were re-checked a few days after. If the purity of positive cell population is below 90%, cells would be performed the second round of sorting. For sorting cell from digested tissue for sequencing, a small proportion of sorted cells were re-loaded to Flow Cytometer to check the purify. Other contaminations were filtered out or specifically labeled based on quality of mRNA abundance and transcription characteristics after sequencing (described in Method).
Gating strategy	For all experiment, scatters (FSC-H>0.5M, SSC-H>0.5M), single cell and live/dead (DAPI- or zombie dye-) were performed to define starting cell population. For sorting TCR expressing hybridoma, target cell population were gated as CD3+ CD4+. For checking hybridoma activation, activated cell population were gated as CD11c- CD3+ CD4+ GFP+. For checking immune cell infiltration, cells were gated as CD45+ CD11b+/- B220+/- CD3+/- TCRb+ TCRrd+ CD4+/- CD8+/-. For sorting T cells from spinal cord or meninges for TCR sequencing, target cell population were gated as CD45+ Thy1.2+ CD4+ or CD8+. For sorting T cells from spinal cord for FACSseq, target cell population were gated as CD45+ CD11b- TCRβ+ CD4+ CD8- GFP+. For checking retrovirus based T cell proliferation, target cells were gated as CD3+ CD4+ GFP+. For checking mRNA based T cell proliferation, target cells were gated as CD11c- CD3+ CD4+. For checking 2D2/ OT-II T cell infiltration of optic nerve, target cells were gated as CD45+ CD3+ CD4+ Vb11+ or CD45+ CD11b- CD3+ TCRb+ CD4+ Vb11+ or Vb5+. For checking the proportion of injected T cells, target cell population were gated as CD45+ CD11b- B220- TCRβ+ Thy1.2+ Thy1.1-. For checking the phenotype of injected T cells, target cell population were gated as CD45+ CD11b- B220- TCRβ+ Thy1.2+ Thy1.1- CD4+ CD8-.

Tick this box to confirm that a figure exemplifying the gating strategy is provided in the Supplementary Information.